

# An analysis of embedded weak discontinuity approaches for the finite element modelling of heterogeneous materials

A. Ortega<sup>a</sup>, E. Roubin<sup>a</sup>, Y. Malecot<sup>a</sup>, L. Daudeville<sup>a</sup>

<sup>a</sup>*Univ. Grenoble Alpes, CNRS, Grenoble INP, 3SR, F-38000 Grenoble, France*

---

## Abstract

This paper analyses in detail the use of the Embedded Finite Element Method (E-FEM) to simulate local material heterogeneities. The work starts by making a short review on the evolution of weak discontinuity models within the E-FEM framework to discuss how they account for the presence of multiple materials within a single element structure. A theoretical basis is introduced through some mathematical weak discontinuity definitions and the Hu-Washizu variational principle, for then establishing a set of requirements for retaining variational and kinematic consistency for any weak discontinuity enhancement proposal. From a general definition of a displacement enhancement field, two particular enhancement functions are derived by considering different consistency requirements: one which has been typically used in previous works and other which truly possesses variational consistency. A discussion is held on enhancement stability properties and the impact to global finite element solution processes. In the end, numerical simulations are made to assess the performance of each of these enhancements on the task of modelling a classical bi-material layered 3D tension problem. The final discussion evaluates both model performance and ease of implementation.

*Keywords:* E-FEM modelling, embedded weak discontinuity, enhanced finite elements, incompatible modes, local heterogeneity modelling, finite element enhancement functions, mixed finite element

---

## 1. Introduction

The numerical modeling of the heterogeneous nature of some materials is important for studying and predicting complex features of their physical behavior, including their mechanical response and resistance under specific conditions.

Typical numerical analysis techniques such as the finite element or finite difference methods generally approach this problem considering homogeneous base domains. This requires a homogenisation procedure for a determined representative patch of the heterogeneous material that is big enough to exhibit the material's behavior as if it were a whole continuum but still small enough to be able to reveal its heterogeneous structure. Such is the basis of representative volume element (RVE) approaches [1, 2].

At some point, every approach following this line will require a realistic modeling of a limited domain on the scale in which the heterogeneities of a given material can be geometrically described in an accurate way. For such multi-scale simulation processes, a classical FEM approach will require an adapted mesh (or at least a specific treatment to it) for the small scale to consistently capture the geometrical distribution of material heterogeneities in such domain. While sophisticated meshing adaptation techniques for heterogeneous objects are still an active subject of study [3, 4], the approach remains computationally expensive and mathematically complicated, depending always on the arbitrary shapes of the different material phases present on the heterogeneous structure. This is specially true when a study requires the analysis of a large amount of heterogeneity distribution samples for a meaningful statistical treatment, such as in the execution of Monte Carlo methods that require repetitive samplings for the homogenisation process [5].

Alternative approaches for the numerical modelling of heterogeneous material domains have emerged, such as Voronoi cell techniques [6], discrete elements for granular rocks [7] or reinforced concrete [8], or the advanced finite element methods [9, 10, 11]. Some of these approaches will focus more on the material interfaces, like the Voronoi cells that make use of mixed 1-D finite elements to represent the presence of different material domains and the strength of the mechanical connection between them. Typically, it is the finite element methods in two or three dimensions that will grant a more meaningful representation of the state of stresses in continuous material models, since they attempt a more direct and accurate geometrical description of material heterogeneities.

In regards to the latter, the *meshfree* or non-adaptive mesh approaches have been introduced as an attractive solution to this modelling problem. To this effect, applications of many advanced FEM techniques can be found, such as the Generalized Finite Element Method (G-FEM) [11], the Extended Finite Element Method (X-FEM) [12], the Base Force Element Method (B-FEM) [13] or the Embedded Finite Element Method (E-FEM) [14], the last one being precisely the scope of study in this work.

It is recognized by the authors of this study that some approaches such as the X-FEM, in the state as they are at the moment of writing, have a broader capacity for the representation of complex multiphase material distributions within a finite element domain than that of the E-FEM element technology. The interest in this work, however, will remain focused on the E-FEM framework. The authors consider worth the effort to keep the advantages of this approach, such as the simplicity and hermeticity of the mathematical enhancements that leave the global finite element solution process practically untouched.

A brief analysis on the evolution of the use of the weak discontinuity model on the E-FEM approach will be presented to the reader in Section 2. A detailed analysis of the theoretical foundations for the definition of weak discontinuity enhancements for the modelling of heterogeneous materials will be introduced in Section 3. This will help to establish a set of basic consistency requirements for defining these enhancements under the light of the Hu-Washizu variational framework. In Section 4, two particular weak discontinuity enhancement functions will be derived based on this consistency analysis and the amount of requirements chosen to be satisfied. The first of them is the one typically managed in the reference E-FEM works, and a second one is proposed to purposefully maximize variational and kinematic consistency.

Finally, basic comparative numerical simulations are made between the weak discontinuity enhancement proposals in Section 5. The analytical solution for a basic heterogeneous model will serve as a reference to assess the performance of the enhancements, as well as any further comments on particular behaviours. A concluding discussion will follow in Section 6, considering all theoretical and practical aspects of the developments presented in this work.

## 2. The role of weak discontinuity enhancements on the E-FEM framework

The use of weak discontinuity enhancements started actually as one of the first embedded finite element approaches for the modelling of shear instability bands, with some pioneering studies paving the way for consolidating the E-FEM approach as a whole [15, 16, 17]. The main idea was to model a shear band through the use of two parallel strain discontinuity lines that would cross a non-adapted mesh, typically having a uniform geometry. The elements having sub-domains enclosed by the shear band would have different constitutive properties to represent the local instability happening inside. It introduces a jump on the strain field, which translates into a sudden change in slope for its corresponding displacement field without breaking its continuity (this is thus the reason of calling it a *weak discontinuity enhancement*). Figure 1 shows an example for a constant stress triangle (CST) element. The localisation band model represented a finite and continuous region of a fracture process.

The weak discontinuity approach for this kind of material failure modelling got diversified afterwards with the introduction of regularization processes [18, 19] to avoid scale dependencies, especially concerning

the problem of setting an arbitrary shear band thickness. Eventually, attention was diverted towards the strong discontinuity enhancement equipped with a discrete post-localisation law as the method of choice for the modelling of internal element fracture on the E-FEM framework [20, 21, 22, 23]. The tendency of this evolution was practically to drive the shear band model thickness to zero while maintaining mathematical and physical coherence on the formulation. This translates the discontinuity to the displacement field directly (thus the reason of naming it a *strong discontinuity*). The strong discontinuity enhancement was indeed proven to be a more pragmatic and robust way to avoid mesh dependencies as possible, granting more objectivity to the approach. Nonetheless, the application of embedded weak discontinuity enhancements for the modelling of shear bands still gathers some interest in recent works, such as ductile material failure simulations under dynamic conditions [24, 25].

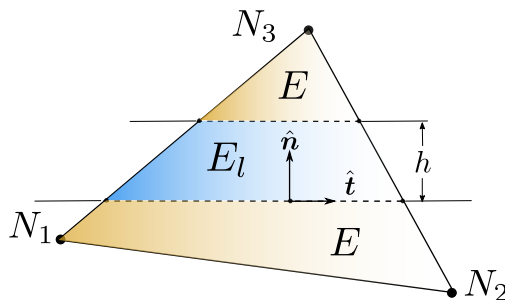


Figure 1: Basic schematic of weak discontinuity enhancements used to represent a shear band within a triangular 2D element having a local frame  $\hat{\mathbf{n}}, \hat{\mathbf{t}}$ . The shear band possesses a set of different (damaged) mechanical properties  $E_l$  while the rest of the element retains its original elastic behavior  $E$ . Note the introduction of a thickness  $d$  characterising the shear band.

The authors of this study consider that the application of weak discontinuity enhancements to model material heterogeneities really started with the works on fracture simulations of cementitious materials on the mesoscale [26, 27, 28]. These developments began by modeling a single weak discontinuity on 1-D beam elements to represent the presence of two different linear elastic stiffness domains coexisting on the same element. The perspective was different to that of Voronoi cell constructions [6] in the sense that no regular inclusion recognition had to be made on a material matrix to assign one beam per interface. A totally random, unstructured 3-D mesh was built with beam elements and a heterogeneity distribution in space was just projected directly onto these. Some elements would fall entirely on the domain of one material phase or other, while others would be found in a region where there was an interface between materials. It is those elements that were enriched with a weak discontinuity enhancement function.

The model was also equipped with a strong discontinuity enhancement at the same location as the weak discontinuity to represent eventual failure and separation of the domains. In this sense, the work was also innovating from the perspective of integrating both discontinuity enhancements for entirely different roles. While this model allowed an explicit use of the weak discontinuity to finally model mesh-independent heterogeneities, no objective state of stresses was described in the domains as no spatially accurate representation of the continuum is possible by only making use of 1-D beam elements.

It was until the work of Roubin [14] that this application of the weak discontinuity model was devised for 3-D elements, inspired on the works in [29, 27]. The main idea was to establish a piece-wise displacement field enrichment that, once being processed through the application of a symmetrical gradient operator  $\nabla^{sym}$ , it would comply with the Maxwell interface strain compatibility conditions [15]. The model counts with one, two or three internal variables characterising the strain jump between materials depending on the dimension of the problem. As his predecessors, Roubin also appended a strong discontinuity enhancement to integrate a fracture model, but only considering a single fracture kinematic mode: normal separation.

This 3-D development was later taken as a base in [30, 31, 32] to perform simulations for heterogeneous rocks and cementitious materials in a similar fashion. A variety of fracture phenomena was explored, such as

plane sliding, crack reclosure and multi-scale analyses, among other developments. Further applications of these ideas can be found in the domain of poromechanics and electromechanics [33, 34]. The use of the weak discontinuity on this format acquired yet more relevance with the work of Stamati et al. [31], where image processing techniques and X-Ray tomography made possible to project realistic heterogeneity distributions coming from actual samples used for experimental campaigns, reaching a new level of predictability and model validation procedures.

This application of the weak discontinuity model for 3-D geometries as seen in the work of Roubin [14] has been taken as the point of departure for the present study. In the next section, the theoretical basis behind it will be scrutinised in detail.

### 3. Theoretical foundations and consistency analysis

The basic construction of a weak discontinuity for the modelling of material heterogeneities starts with the assumption that a heterogeneous displacement field  $\mathbf{u}$ , referred from now on to as the *physical* displacement, can be expressed as the composition of an average, homogenized base field  $\bar{\mathbf{u}}$  and a field enhancement  $\tilde{\mathbf{u}}$  carrying the mathematical weak discontinuity:

$$\mathbf{u} = \bar{\mathbf{u}} + \tilde{\mathbf{u}} \quad (1)$$

Figure 2 illustrates a typical dual material partition for a 4-node tetrahedral element in domains  $\Omega^+$ ,  $\Omega^-$  with a boundary  $\partial\Omega$  and having a plane  $\Gamma_d$  as an interface. The base work in [14, 35] considers linear elastic properties for each domain such as Young moduli  $E^+$ ,  $E^-$  and Poisson ratios  $\nu^+$ ,  $\nu^-$ . A local coordinate system  $(\hat{\mathbf{n}}, \hat{\mathbf{t}}, \hat{\mathbf{m}})$  defines the orientation of the material interface, having  $\hat{\mathbf{n}}$  as the unit vector normal to  $\Gamma_d$ .

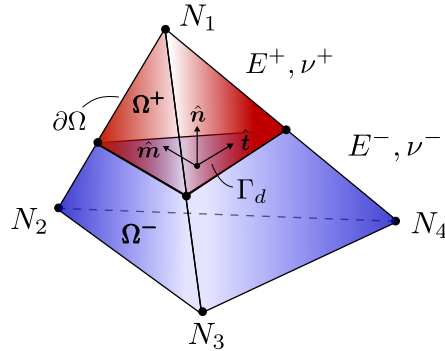


Figure 2: Basic schematic of a weak discontinuity in 3-D for the modelling of material heterogeneities within a tetrahedral element

The homogeneous base field  $\bar{\mathbf{u}}$  is determined entirely by the displacement of the boundary nodes and the natural interpolation functions of the element. The definition of the field  $\tilde{\mathbf{u}}$  is determined by internal variables keeping in mind that its corresponding strain function should introduce the strain jump associated with the change of material domains. The strain fields, as second order tensors, are obtained through a symmetric gradient operator  $\nabla^s(\bullet) = \frac{1}{2} [\nabla(\bullet)^T + \nabla(\bullet)]$ :

$$\boldsymbol{\varepsilon} = \nabla^s \mathbf{u} = \nabla^s \bar{\mathbf{u}} + \nabla^s \tilde{\mathbf{u}} = \bar{\boldsymbol{\varepsilon}} + \tilde{\boldsymbol{\varepsilon}} \quad (2a)$$

$$\boldsymbol{\varepsilon}^+ = \bar{\boldsymbol{\varepsilon}} + \tilde{\boldsymbol{\varepsilon}}^+, \quad \mathbf{x} \in \Omega^+ \quad (2b)$$

$$\boldsymbol{\varepsilon}^- = \bar{\boldsymbol{\varepsilon}} + \tilde{\boldsymbol{\varepsilon}}^-, \quad \mathbf{x} \in \Omega^- \quad (2c)$$

where a distinction has been done between the strain fields on the  $\Omega^+$  and  $\Omega^-$  domains at each side of  $\Gamma_d$ . Note that the base field  $\bar{\boldsymbol{\varepsilon}}$  remains invariant by the definition of  $\bar{\mathbf{u}}$ .

### 3.1. Enhancement requirements and variational analysis

To retain kinematic and variational consistency, the weak discontinuity model has to comply with certain requirements through both displacement and strain fields. The approach in this study will be to determine the possible function space for the enhanced displacement field by introducing and applying these constraints, also noting the set of constraints effectively considered in the work of [14] that shapes the most typical choice for it in those works.

From now on, the analysis will take place on the local reference frame  $(\hat{\mathbf{n}}, \hat{\mathbf{t}}, \hat{\mathbf{m}})$  unless stated otherwise. Its coordinate variables will be denoted as  $\xi, \eta, \zeta$ .

The most basic constraint pertains the physical displacement field  $\mathbf{u}$ : it shall not lose continuity through the material interface. Given that the base field  $\bar{\mathbf{u}}$  is already continuous by definition, this implies that that enhanced displacement  $\tilde{\mathbf{u}}$  also has to be continuous:

#### **Enhancement requirement 1: displacement continuity**

$$\tilde{\mathbf{u}}^+ \Big|_{\Gamma_d} = \tilde{\mathbf{u}}^- \Big|_{\Gamma_d} \quad (3)$$

The next involves an analysis of the strain field and the definition of the strain discontinuity jump. A strain discontinuity jump  $\Delta\tilde{\boldsymbol{\varepsilon}}$  is defined the difference of strain fields  $\tilde{\boldsymbol{\varepsilon}}^+$  and  $\tilde{\boldsymbol{\varepsilon}}^-$  at the material interface  $\Gamma_d$ , resulting also in a second order tensor:

$$\Delta\tilde{\boldsymbol{\varepsilon}} = \tilde{\boldsymbol{\varepsilon}}^+ \Big|_{\Gamma_d} - \tilde{\boldsymbol{\varepsilon}}^- \Big|_{\Gamma_d} = \begin{bmatrix} \Delta\tilde{\varepsilon}_{nn} & \Delta\tilde{\varepsilon}_{nt} & \Delta\tilde{\varepsilon}_{nm} \\ \text{sym} & \Delta\tilde{\varepsilon}_{tt} & \Delta\tilde{\varepsilon}_{tm} \\ \text{sym} & \text{sym} & \Delta\tilde{\varepsilon}_{mm} \end{bmatrix} \quad (4)$$

The components of the strain jump  $\Delta\tilde{\boldsymbol{\varepsilon}}$  are not obliged to respect full continuity as their parent displacement field, but must still comply with Maxwell strain compatibility conditions [15] to be coherent with it. For this, the projection of  $\Delta\tilde{\boldsymbol{\varepsilon}}$  on the normal direction  $\hat{\mathbf{n}}$  will be allowed to be free of constraints, while all other unrelated components of the tensor will be driven down to zero. Recall that in a local coordinate setting, the projections can be easily obtained by just extracting the line-column corresponding to a given direction within the tensor. Thus:

$$\begin{aligned} \Delta\tilde{\boldsymbol{\varepsilon}} \cdot \hat{\mathbf{n}} &= [\Delta\tilde{\varepsilon}_{nn} \quad \Delta\tilde{\varepsilon}_{nt} \quad \Delta\tilde{\varepsilon}_{nm}]^T \neq \mathbf{0} \\ \Delta\tilde{\varepsilon}_{tt} &= \Delta\tilde{\varepsilon}_{tm} = \Delta\tilde{\varepsilon}_{mm} = 0 \end{aligned} \quad (5)$$

This leaves the strain jump tensor  $\Delta\tilde{\boldsymbol{\varepsilon}}$  with only three active components  $\Delta\tilde{\varepsilon}_{nn}$ ,  $\Delta\tilde{\varepsilon}_{nt}$ ,  $\Delta\tilde{\varepsilon}_{nm}$ . These will be redefined as  $[\varepsilon]_n$ ,  $[\varepsilon]_t$  and  $[\varepsilon]_m$ , respectively. These are indeed the internal variables that define the weak discontinuity model. With this, a new enhancement requirement is defined:

#### **Enhancement requirement 2: strain jump**

$$\Delta\tilde{\boldsymbol{\varepsilon}} = \tilde{\boldsymbol{\varepsilon}}^+ \Big|_{\Gamma_d} - \tilde{\boldsymbol{\varepsilon}}^- \Big|_{\Gamma_d} = \begin{bmatrix} [\varepsilon]_n & [\varepsilon]_t & [\varepsilon]_m \\ [\varepsilon]_t & 0 & 0 \\ [\varepsilon]_m & 0 & 0 \end{bmatrix} \quad (6)$$

The requirements to follow need considerations coming from the variational analysis. As in [36, 14, 30] and in most of other works on the E-FEM framework, the Hu-Washizu variational principle is chosen due

to its flexibility to handle element field enhancements through the independence of displacement, strain and stress fields:

$$\int_{\Omega} \partial \delta \mathbf{u}^t \boldsymbol{\sigma} dV - \int_{\Omega} \delta \mathbf{u}^t \mathbf{f}_b dV - \int_{\partial\Omega} \delta \mathbf{u}^t \mathbf{t} dA = 0 \quad (7a)$$

$$\int_{\Omega_e} \delta \boldsymbol{\sigma}^t (\partial \mathbf{u} - \boldsymbol{\varepsilon}) dV = 0 \quad (7b)$$

$$\int_{\Omega_e} \delta \boldsymbol{\varepsilon}^t (\boldsymbol{\sigma}(\boldsymbol{\varepsilon}) - \boldsymbol{\sigma}) dV = 0 \quad (7c)$$

where the real fields have been denoted as  $(\mathbf{u}, \boldsymbol{\varepsilon}, \boldsymbol{\sigma})$  and the field variations (or *virtual* fields) as  $(\delta \mathbf{u}, \delta \boldsymbol{\varepsilon}, \delta \boldsymbol{\sigma})$ , having a boundary traction vector  $\mathbf{t}$  and body forces  $\mathbf{f}_b$ . It's important to note that the real stress field  $\boldsymbol{\sigma}$ , in general, is different from the stress coming from constitutive law calculations  $\boldsymbol{\sigma}(\boldsymbol{\varepsilon})$ . The same can be said from the real strain field  $\boldsymbol{\varepsilon}$  and  $\partial \mathbf{u}$ , where  $\partial$  is a field gradient operator. A Voigt vector notation has been already implied for all fields involved in the presentation of Eqs. 7a-7c.

All fields are independent from each other, in the sense that they do not have to necessarily follow direct gradient relations such as in Eq. 2a. This is, the Hu-Washizu variational principle allows for flexible field discretization strategies. However, the fields should retain enough physical meaningfulness to be able to correctly model the phenomenon in question. Authors working on this framework generally choose a discretisation strategy as to render the model as manageable and efficient as possible sacrificing the minimal amount of mechanical representation quality. This choice also considers the ease of an integration process with other models that might have a similar field discretisation approach (such as a strong discontinuity model).

The displacement and displacement variation fields  $\mathbf{u}$ ,  $\delta \mathbf{u}$  are commonly discretized taking only the standard displacement field  $\bar{\mathbf{u}}$ :

$$\mathbf{u} = \bar{\mathbf{u}} = \mathbf{N} \mathbf{d} \quad (8a)$$

$$\delta \mathbf{u} = \mathbf{N} \delta \mathbf{d} \quad (8b)$$

with  $\mathbf{N}$  as a standard interpolation matrix and  $\mathbf{d}$  the standard nodal displacement vector.  $\delta \mathbf{d}$  is the corresponding variation. This strategy means that only the field  $\bar{\mathbf{u}}$  is used for describing node positions and imposing boundary conditions. In such case, it should be clear that, in order to ensure that  $\mathbf{d}$  retains the correct nodal information, the field  $\bar{\mathbf{u}}$  should have the same value as  $\mathbf{u}$  at the boundaries  $\partial\Omega$  of all the element (i.e. the nodes on it):

$$\mathbf{u}|_{\partial\Omega} = \bar{\mathbf{u}}|_{\partial\Omega} \quad (9)$$

Given that we already have a definition as stated in Eq. 1, this implies:

$$\mathbf{u}|_{\partial\Omega} = \bar{\mathbf{u}}|_{\partial\Omega} + \tilde{\mathbf{u}}|_{\partial\Omega} \Rightarrow \tilde{\mathbf{u}}|_{\partial\Omega} = 0 \quad (10)$$

This analysis defines the next constraint for the weak discontinuity model:

**Enhancement requirement 3: null value on borders**

$$\tilde{\mathbf{u}}|_{\mathbf{x}=\mathbf{x}_i} = 0, \quad i = 1, 2, \dots, N \quad (11)$$

where  $\mathbf{x}_i$  are nodal positions and  $N$  is the number of nodes of the element. This requirement stands as the most overlooked in the current literature of this family of formulations applied to the modelling of material

heterogeneities. It is also the one that will make a significant difference in the enhancement function shape with respect to the one used in typical heterogeneous E-FEM studies.

Going forward with the discretisation strategy, the domain dependent strain field  $\boldsymbol{\varepsilon}$  and its variation  $\delta\boldsymbol{\varepsilon}$  conserve all kinematics description terms as stated in Eqs. 2a-2b. Their enhanced sections ( $\tilde{\boldsymbol{\varepsilon}}$  and  $\delta\tilde{\boldsymbol{\varepsilon}}$ , respectively), which depend on the internal variables  $[\boldsymbol{\varepsilon}]_n$ ,  $[\boldsymbol{\varepsilon}]_t$ ,  $[\boldsymbol{\varepsilon}]_m$ , are stated through the definition of a *weak discontinuity vector*  $[[\boldsymbol{\varepsilon}]] = [[\boldsymbol{\varepsilon}]_n \quad [\boldsymbol{\varepsilon}]_t \quad [\boldsymbol{\varepsilon}]_m]^T$  and its variation  $\delta[[\boldsymbol{\varepsilon}]]$ . This discretisation strategy also allows the opportunity to use different interpolation matrices  $\mathbf{G}_w^\pm$ ,  $\mathbf{G}_w^{*\pm}$  for the real and variation enhancements, respectively:

$$\boldsymbol{\varepsilon} = \begin{cases} \mathbf{B}\mathbf{d} + \mathbf{G}_w^+ [[\boldsymbol{\varepsilon}]] & \mathbf{x} \in \Omega^+ \\ \mathbf{B}\mathbf{d} + \mathbf{G}_w^- [[\boldsymbol{\varepsilon}]] & \mathbf{x} \in \Omega^- \end{cases} \quad (12a)$$

$$\delta\boldsymbol{\varepsilon} = \begin{cases} \mathbf{B}\delta\mathbf{d} + \mathbf{G}_w^{*+} \delta[[\boldsymbol{\varepsilon}]] & \mathbf{x} \in \Omega^+ \\ \mathbf{B}\delta\mathbf{d} + \mathbf{G}_w^{*-} \delta[[\boldsymbol{\varepsilon}]] & \mathbf{x} \in \Omega^- \end{cases} \quad (12b)$$

Note that, until now, no specific form for  $\mathbf{G}_w^\pm$ ,  $\mathbf{G}_w^{*\pm}$  has been still assigned. In the original work of Roubin [14], it is actually assumed that  $\mathbf{G}_w^\pm = \mathbf{G}_w^{*\pm}$ . The reason for this choice will be explained shortly.

The stress field  $\boldsymbol{\sigma}$  and its variation  $\delta\boldsymbol{\sigma}$  are just interpolated using single independent stress vectors  $\mathbf{s}$  and  $\delta\mathbf{s}$  through the use of interpolation matrices  $\mathbf{S}$  and  $\mathbf{S}^*$ , respectively:

$$\boldsymbol{\sigma} = \mathbf{S}\mathbf{s} \quad (13a)$$

$$\delta\boldsymbol{\sigma} = \mathbf{S}^*\delta\mathbf{s}, \quad (13b)$$

The definition for the stress field coming from the constitutive law  $\boldsymbol{\sigma}(\boldsymbol{\varepsilon})$  is based on the assumption that each of the material domains possesses its own linear elastic constitutive law considering separate second order linear elastic constitutive tensors  $\mathbf{C}^+$  and  $\mathbf{C}^-$ . These linear operators act upon different regions of the *real* strain field  $\boldsymbol{\varepsilon}$ . The definition for this stress field is thus devised as:

$$\boldsymbol{\sigma}(\boldsymbol{\varepsilon}) = \begin{cases} \mathbf{C}^+ (\mathbf{B}\mathbf{d} + \mathbf{G}_w^+ [[\boldsymbol{\varepsilon}]]) & \mathbf{x} \in \Omega^+ \\ \mathbf{C}^- (\mathbf{B}\mathbf{d} + \mathbf{G}_w^- [[\boldsymbol{\varepsilon}]]) & \mathbf{x} \in \Omega^- \end{cases} \quad (14)$$

It should be emphasized that while the constitutive stress  $\boldsymbol{\sigma}(\boldsymbol{\varepsilon})$  is by default a domain-dependent definition, the *real* stress field  $\boldsymbol{\sigma}$  is not necessarily obliged to follow the same characteristics.

Having set a discretisation strategy, the variational analysis takes place by using all previous equations to develop the Hu-Washizus system through Eqs. 7a-7c. For instance, after working Eq. 7b and considering that independence of  $[[\boldsymbol{\varepsilon}]]$  as well as the fact that the variation vector  $\delta\mathbf{s}$  is to remain arbitrary, it follows that:

$$\delta\mathbf{s}^t \int_{\Omega_e} \mathbf{S}^{*t} \mathbf{G}_w^\pm dV [[\boldsymbol{\varepsilon}]] = \mathbf{0} \Rightarrow \int_{\Omega_e} \mathbf{S}^{*t} \mathbf{G}_w^\pm dV = \mathbf{0} \quad (15)$$

Eq. 15 demands orthogonality between the virtual stress interpolation matrix  $\mathbf{S}^*$  and the enhancement matrix operators  $\mathbf{G}_w^\pm$  on each respective subvolume  $V^+$ ,  $V^-$ . Since the matrix  $\mathbf{S}^*$  does not represent any kind constraint on any real field in the framework, most authors just take this relation as granted assuming that for any convenient choice of shape for the *real*  $\mathbf{G}_w^\pm$  matrix operators, there will always exist a definition for  $\mathbf{S}^*$  complex enough to satisfy Eq. 15. Indeed this is case for usual enhancement function proposals, but the demonstration will not be done on the present work. It will be only stressed that, since  $\mathbf{S}^*$  will be defined following exclusively the structure of a chosen  $\mathbf{G}_w^\pm$ , it is clear that virtual stresses and real stresses will be interpolated in an asymmetrical fashion. Therefore, the framework already departs from this point from a classical Bubnov-Galerkin variational approach to a Petrov-Galerkin one.

Next, the works with Eq. 7c lead to two independent equations thanks again to the arbitrary nature of  $\delta \mathbf{d}$  and  $\delta [|\boldsymbol{\varepsilon}|]$ :

$$\delta \mathbf{d}^t \int_{\Omega_e} \mathbf{B}^t (\boldsymbol{\sigma} (\boldsymbol{\varepsilon}) - \mathbf{S} \mathbf{s}) dV + \delta [|\boldsymbol{\varepsilon}|]^t \int_{\Omega_e} \mathbf{G}_w^{*\pm t} (\boldsymbol{\sigma} (\boldsymbol{\varepsilon}) - \mathbf{S} \mathbf{s}) dV = 0 \quad (16a)$$

$$\rightarrow \delta \mathbf{d}^t \int_{\Omega_e} \mathbf{B}^t (\boldsymbol{\sigma} (\boldsymbol{\varepsilon}) - \mathbf{S} \mathbf{s}) dV = 0 \rightarrow \int_{\Omega} \mathbf{B}^t \boldsymbol{\sigma} (\boldsymbol{\varepsilon}) dV = \int_{\Omega} \mathbf{B}^t \mathbf{S} \mathbf{s} dV \quad (16b)$$

$$\rightarrow \delta [|\boldsymbol{\varepsilon}|]^t \int_{\Omega_e} \mathbf{G}_w^{*\pm t} (\boldsymbol{\sigma} (\boldsymbol{\varepsilon}) - \mathbf{S} \mathbf{s}) dV = 0 \rightarrow \int_{\Omega} \mathbf{G}_w^{*\pm t} \boldsymbol{\sigma} (\boldsymbol{\varepsilon}) dV = \int_{\Omega} \mathbf{G}_w^{*\pm t} \mathbf{S} \mathbf{s} dV \quad (16c)$$

Eq. 16b is the only relation in the framework that establishes an explicit connection between real and constitutive stresses. It stands as a weak equality involving a known standard interpolation gradient matrix  $\mathbf{B}$ . In the case that the choices in the weak discontinuity model render the shapes (*e.g.*, polynomial order) of  $\boldsymbol{\sigma} (\boldsymbol{\varepsilon})$  and  $\boldsymbol{\sigma}$  to be the same, then a strong equality between the fields will hold. This also implies that the real stresses  $\boldsymbol{\sigma}$  will have to be domain dependent as  $\boldsymbol{\sigma} (\boldsymbol{\varepsilon})$ . For other cases, notably for an assumed constant real stress field, a volume-averaged expression can be used for its calculation:

$$\mathbf{s} = \frac{1}{V_e} \int_{\Omega} \boldsymbol{\sigma} (\boldsymbol{\varepsilon}) dV, \quad (17)$$

where the shape, order or domain distribution of  $\boldsymbol{\sigma} (\boldsymbol{\varepsilon})$  is irrelevant.

For working Eq. 16c, authors commonly *assume* that both left and right sides can be set to zero, creating orthogonality constraints. On the right side, given that the *real* stress interpolation matrix  $\mathbf{S}$  is fixed based on *real* node data, the orthogonality defines the structure of  $\mathbf{G}_w^{*\pm t}$ . In general we will have:

$$\int_{\Omega_e} \mathbf{G}_w^{*\pm T} \mathbf{S} \mathbf{s} dV = \int_{\Omega^+} \mathbf{G}_w^{*+T} \mathbf{S} dV \mathbf{s}^+ + \int_{\Omega^-} \mathbf{G}_w^{*-T} \mathbf{S} dV \mathbf{s}^- = 0 \quad (18)$$

Depending on the *chosen* form for  $\boldsymbol{\sigma}$ , the definition for the  $\mathbf{G}_w^{*\pm T}$  operators will change attending to Eq. 18. Additionally, there is the requirement of passing a finite element *patch test* [29, 37]. The patch test states that it should be possible to satisfy all variational equations for a constant real stress field *regardless* of the form chosen for this field in the first place. In other words, Eq. 18 must be satisfied for **both** a case in which the interpolation matrix  $\mathbf{S}$  is the identity matrix and the case in which  $\mathbf{S}$  corresponds to the shape functions truly desired to describe the stress field. With this in mind, it will be required to have  $\mathbf{s}^+ = \mathbf{s}^- = \mathbf{s}$  for validating the case of some uniform and arbitrary-valued  $\mathbf{s}$  over all the element domain  $\Omega_e$ . This yields another requirement for the weak discontinuity model enhancement, even if this part of the discussion focuses on its virtual definition:

#### **Enhancement requirement 4: Patch Test**

$$\int_{\Omega^+} \mathbf{G}_w^{*+T} dV + \int_{\Omega^-} \mathbf{G}_w^{*-T} dV = \mathbf{0} \quad (19)$$

For instance, the works in [14, 35] take the simplest approach for a tetrahedron element, which is to assume a constant real stress field. In this case, the patch test requirement actually *obliges* the entire real stress field to be constant and unique through all the element. Thus, it will have to be always calculated using a volume average (Eq. 17). On the other hand, this lowers the burden of also having to satisfy Eq. 18 for a higher order  $\mathbf{S}$ . This leaves Eq. 19 as the only requirement for  $\mathbf{G}_w^{*\pm}$ , which allows the possibility to make constant matrix definitions, yielding:

$$V^+ \mathbf{G}_w^{*+} + V^- \mathbf{G}_w^{*-} = \mathbf{0} \quad (20)$$

Setting the left side of Eq. 16c to zero brings the final relation for calculating the weak discontinuity internal variables  $[\varepsilon]_n$ ,  $[\varepsilon]_t$ ,  $[\varepsilon]_m$  as a function of a displacement input  $\mathbf{d}$ . This is, if a definite shape for all weak discontinuity enhancement matrix operators  $\mathbf{G}_w^\pm$  and  $\mathbf{G}_w^{*\pm}$  have been established at this point. Eq. 14 can be used to develop:

$$\int_{\Omega^+} \mathbf{G}_w^{*+T} \mathbf{C}^+ (\mathbf{B}\mathbf{d} + \mathbf{G}_w^+ [[\varepsilon]]) dV + \int_{\Omega^-} \mathbf{G}_w^{*-T} \mathbf{C}^- (\mathbf{B}\mathbf{d} + \mathbf{G}_w^- [[\varepsilon]]) dV = \mathbf{0} \quad (21a)$$

$$\mathbf{K}_{wb}\mathbf{d} + \mathbf{K}_{ww} [[\varepsilon]] = \mathbf{0} \quad (21b)$$

$$\mathbf{K}_{wb} = \int_{\Omega^+} \mathbf{G}_w^{*+T} \mathbf{C}^+ \mathbf{B} dV + \int_{\Omega^-} \mathbf{G}_w^{*-T} \mathbf{C}^- \mathbf{B} dV \quad (21c)$$

$$\mathbf{K}_{ww} = \int_{\Omega^+} \mathbf{G}_w^{*+T} \mathbf{C}^+ \mathbf{G}_w^+ dV + \int_{\Omega^-} \mathbf{G}_w^{*-T} \mathbf{C}^- \mathbf{G}_w^- dV \quad (21d)$$

$$[[\varepsilon]] = \mathbf{K}_{ww}^{-1} \mathbf{K}_{wb} \mathbf{d}, \quad (21e)$$

where specific enhancement stiffness matrices  $\mathbf{K}_{wb}$ ,  $\mathbf{K}_{ww}$  have been defined.

The direct equality between both sides of equation Eq. 16c brings additional information on some internal constraints for the stress fields that will emerge implicitly without impacting further enhancement definitions on the weak discontinuity model overall. The implications are interesting to know but are not operationally useful. For instance, if constant matrix definitions are done for the virtual  $\mathbf{G}_w^{*\pm}$  operators, one can use Eq. 20 to express everything a function of the  $\mathbf{G}_w^+$  operator, isolate and finally reach:

$$\frac{1}{V^+} \int_{\Omega^+} \boldsymbol{\sigma}^+(\boldsymbol{\varepsilon}) dV = \frac{1}{V^-} \int_{\Omega^-} \boldsymbol{\sigma}^-(\boldsymbol{\varepsilon}) dV \quad (22)$$

If enhancements are defined in such a way that the constitutive stress fields are constant on each domain, then Eq. 22 practically dictates a strong equality and uniformity of the constitutive stress fields in all the element. At the same time, the strain fields are *assured* to be different on each domain by definition. While this emerging equality might appear counter-intuitive to the reader, this would resemble a very simplistic situation such as in a couple of springs connected in series, where the strain is different but the force through them is exactly the same. Indeed, Eq. 22 has been observed to hold for a large number of elements during actual numerical simulations based on the formulation of Roubin [14] for large models managed in the works of Stamati et al. [31].

#### 4. Weak discontinuity enhancement proposals

Now that all relevant constraints for defining weak enhancement functions have been introduced, a particularisation of the model will take place, deriving two different enhancement field functions considering slightly different ways of achieving the satisfaction of consistency requirements. For the sake of simplicity and coherence with the background literature, a linear tetrahedron will be set as the base element from now on. For now, it will be assumed that a constant stress field  $\boldsymbol{\sigma}$  is sought.

##### 4.1. Typical enhancement analysis

Authors managing the modelling approach in [14, 35] decide to make the weak discontinuity enhancement completely symmetrical by letting  $\mathbf{G}_w^\pm = \mathbf{G}_w^{*\pm}$ . This automatically renders the weak discontinuity model variationally symmetric at the expense of removing the flexibility of having a virtual enhancement with different characteristics. At the same time, only requirements 1, 2 and 4 (Eqs. 3, 6, 19) are explicitly imposed to this unique enhancement function. Instead of requirement 3 (Eq. 11), a general zero reference for the enhancement is set at the interface plane  $\Gamma_d$ . This last imposition is absolutely unrelated to any considerations on variational consistency. This line of approach also chooses the simplest definition for the model: a linear field  $\tilde{\mathbf{u}}$  and therefore constant operators  $\mathbf{G}_w^\pm$ .

Considering these restrictions, it will be demonstrated that the possible function space for  $\tilde{\mathbf{u}}$  reduces to a unique expression. Let the following linear definitions for the piece-wise enhanced displacement field be:

$$\tilde{\mathbf{u}}^+ = \mathbf{a}^+ + \mathbf{b}^+\xi + \mathbf{c}^+\eta + \mathbf{d}^+\zeta \quad (23a)$$

$$\tilde{\mathbf{u}}^- = \mathbf{a}^- + \mathbf{b}^-\xi + \mathbf{c}^-\eta + \mathbf{d}^-\zeta \quad (23b)$$

where each vector has components contributing to each local direction  $(\hat{\mathbf{n}}, \hat{\mathbf{t}}, \hat{\mathbf{m}})$ , *e.g.*,  $\tilde{\mathbf{u}}^+ = [\tilde{u}_n^+ \ \tilde{u}_t^+ \ \tilde{u}_m^+]^T$ . The goal is to particularize the vectors  $\mathbf{a}^\pm, \mathbf{b}^\pm, \mathbf{c}^\pm, \mathbf{d}^\pm$  as a function of basic element data and the weak discontinuity variables  $[[\varepsilon]]_n, [[\varepsilon]]_t$  and  $[[\varepsilon]]_m$ . In local coordinates, it is not hard to see that the interface plane  $\Gamma_d$  is simply described by the equation  $\xi = 0$ . This eases the application of requirement 1:

$$\tilde{\mathbf{u}}^+ \Big|_{\xi=0} = \tilde{\mathbf{u}}^- \Big|_{\xi=0} \quad (24a)$$

$$\mathbf{a}^+ + \mathbf{c}^+\eta + \mathbf{d}^+\zeta = \mathbf{a}^- + \mathbf{c}^-\eta + \mathbf{d}^-\zeta \quad (24b)$$

$$\Rightarrow \mathbf{a}^+ = \mathbf{a}^- = \mathbf{a}, \quad \mathbf{c}^+ = \mathbf{c}^- = \mathbf{c}, \quad \mathbf{d}^+ = \mathbf{d}^- = \mathbf{d} \quad (24c)$$

where the  $\pm$  will be omitted from now on in all coefficients  $\mathbf{a}, \mathbf{c}, \mathbf{d}$ .

The strain jump requirement (Eq. 6) requires the calculation of the symmetric gradients on each part of the enhanced displacement field:

$$\tilde{\boldsymbol{\varepsilon}}^+ - \tilde{\boldsymbol{\varepsilon}}^- = \begin{bmatrix} [[\varepsilon]]_n & [[\varepsilon]]_t & [[\varepsilon]]_m \\ [[\varepsilon]]_t & 0 & 0 \\ [[\varepsilon]]_m & 0 & 0 \end{bmatrix} \quad (25a)$$

$$\tilde{\boldsymbol{\varepsilon}}^\pm = \begin{bmatrix} u_{n,\xi}^\pm & \frac{1}{2}(u_{n,\eta}^\pm + u_{t,\xi}^\pm) & \frac{1}{2}(u_{n,\zeta}^\pm + u_{m,\xi}^\pm) \\ \text{sym} & u_{t,\eta}^\pm & \frac{1}{2}(u_{t,\zeta}^\pm + u_{m,\eta}^\pm) \\ \text{sym} & \text{sym} & u_{m,\zeta}^\pm \end{bmatrix} = \begin{bmatrix} b_n^\pm & \frac{1}{2}(c_n + b_t^\pm) & \frac{1}{2}(d_n + b_m^\pm) \\ \text{sym} & c_t & \frac{1}{2}(d_t + c_m) \\ \text{sym} & \text{sym} & d_m \end{bmatrix} \quad (25b)$$

$$\tilde{\boldsymbol{\varepsilon}}^+ - \tilde{\boldsymbol{\varepsilon}}^- = \begin{bmatrix} b_n^+ - b_n^- & \frac{1}{2}(b_t^+ - b_t^-) & \frac{1}{2}(b_m^+ - b_m^-) \\ \frac{1}{2}(b_t^+ - b_t^-) & 0 & 0 \\ \frac{1}{2}(b_m^+ - b_m^-) & 0 & 0 \end{bmatrix} \quad (25c)$$

$$\Rightarrow [[\boldsymbol{\varepsilon}]] = \begin{bmatrix} [[\varepsilon]]_n \\ [[\varepsilon]]_t \\ [[\varepsilon]]_m \end{bmatrix} = \begin{bmatrix} b_n^+ - b_n^- \\ \frac{1}{2}(b_t^+ - b_t^-) \\ \frac{1}{2}(b_m^+ - b_m^-) \end{bmatrix} \quad (25d)$$

Here, the results of Eq. 24c have been used. Note that for this reason, the zeros required in the strain jump matrix are produced naturally.

The application of the patch test (Eq. 19) becomes easier if both sides of Eq. 20 are multiplied (contracted) by the weak discontinuity variable vector  $[[\boldsymbol{\varepsilon}]]$  to recover enhanced strain fields, but in vector format:

$$V^+ \underbrace{\mathbf{G}_w^+ [[\boldsymbol{\varepsilon}]]}_{\tilde{\boldsymbol{\varepsilon}}^+} + V^- \underbrace{\mathbf{G}_w^- [[\boldsymbol{\varepsilon}]]}_{\tilde{\boldsymbol{\varepsilon}}^-} = \mathbf{0} [[\boldsymbol{\varepsilon}]] = \mathbf{0} \quad (26a)$$

$$V^+ \begin{bmatrix} b_n^+ \\ c_t \\ d_m \\ \frac{1}{2}(c_n + b_t^+) \\ \frac{1}{2}(d_t + c_m) \\ \frac{1}{2}(d_n + b_m^+) \end{bmatrix} = -V^- \begin{bmatrix} b_n^- \\ c_t \\ d_m \\ \frac{1}{2}(c_n + b_t^-) \\ \frac{1}{2}(d_t + c_m) \\ \frac{1}{2}(d_n + b_m^-) \end{bmatrix} \quad (26b)$$

$$\Rightarrow c_t = d_m = 0 \quad (26c)$$

Afterwards, the original idea for this formulation coming from Markovic [29] involves the imposition of a requirement that is *not mandatory* for variational consistency. The enhanced displacement  $\tilde{\mathbf{u}}$  is prescribed with a value of zero through all the interface plane ( $\xi = 0$ ). While Markovic did never reveal any particular reasons for this decision in his research, it is later found in this work through further mathematical analysis (Sections 4.3, 4.4, 4.5) that this constraint provides some operational benefits to the framework. Indeed, the imposition of a zero enhanced displacement reference at  $\Gamma_d$  is an aggressive constraint that will simplify the enhancement function to a great extent:

$$u^+|_{\xi=0} = u^-|_{\xi=0} = 0 \quad (27a)$$

$$\begin{bmatrix} a_n \\ a_t \\ a_m \end{bmatrix} + \begin{bmatrix} c_n \\ 0 \\ c_m \end{bmatrix} \eta + \begin{bmatrix} d_n \\ d_t \\ 0 \end{bmatrix} \zeta = \begin{bmatrix} 0 \\ 0 \\ 0 \end{bmatrix} \quad (27b)$$

$$\Rightarrow \begin{bmatrix} a_n \\ a_t \\ a_m \end{bmatrix} = \begin{bmatrix} 0 \\ 0 \\ 0 \end{bmatrix}, \quad \begin{bmatrix} c_n \\ 0 \\ c_m \end{bmatrix} = \begin{bmatrix} 0 \\ 0 \\ 0 \end{bmatrix}, \quad \begin{bmatrix} d_n \\ d_t \\ 0 \end{bmatrix} = \begin{bmatrix} 0 \\ 0 \\ 0 \end{bmatrix} \quad (27c)$$

It should not be forgotten that this condition *is not* a replacement of requirement 3 (Eq. 11). With these results and the expressions coming from the application of the patch test requirement (Eq. 26b), one can calculate the  $\mathbf{b}$  coefficients directly as a function of weak discontinuity internal variables:

$$b_n^+ = \frac{V^-}{V} [\varepsilon]_n, \quad b_t^+ = 2 \frac{V^-}{V} [\varepsilon]_t, \quad b_m^+ = 2 \frac{V^-}{V} [\varepsilon]_m, \quad (28a)$$

$$b_n^- = -\frac{V^+}{V} [\varepsilon]_n, \quad b_t^- = -2 \frac{V^+}{V} [\varepsilon]_t, \quad b_m^- = -2 \frac{V^+}{V} [\varepsilon]_m, \quad (28b)$$

In the end, the enhancement function reduces to just a set of  $\mathbf{b}$  coefficients multiplying the coordinate  $\xi$ , which is the normal distance from the interface plane  $\Gamma_d$ :

$$\begin{bmatrix} \tilde{u}_n^\pm \\ \tilde{u}_t^\pm \\ \tilde{u}_m^\pm \end{bmatrix} = \begin{bmatrix} b_n^\pm \\ b_t^\pm \\ b_m^\pm \end{bmatrix} \xi = \pm \frac{V^\mp}{V} \begin{bmatrix} [\varepsilon]_n \\ 2 [\varepsilon]_t \\ 2 [\varepsilon]_m \end{bmatrix} \xi \quad (29a)$$

$$\Rightarrow \tilde{\mathbf{u}}^\pm = \pm \frac{V^\mp}{V} \xi ([\varepsilon]_n \hat{\mathbf{n}} + 2 [\varepsilon]_t \hat{\mathbf{t}} + 2 [\varepsilon]_m \hat{\mathbf{m}}) \quad (29b)$$

If this expression is reverted to global coordinates, the original weak discontinuity enhancement version as used in Roubin [14] is recovered:

***Weak discontinuity enhancement: typical definition***

$$\tilde{\mathbf{u}} = \Theta \hat{\mathbf{n}} \cdot (\mathbf{x} - \mathbf{x}_{\Gamma_d}) ([\varepsilon]_n \hat{\mathbf{n}} + 2 [\varepsilon]_t \hat{\mathbf{t}} + 2 [\varepsilon]_m \hat{\mathbf{m}}) \quad (30)$$

$$\Theta = \begin{cases} \Theta^+ = \frac{V^-}{V} & \mathbf{x} \in \Omega^+ \\ \Theta^- = -\frac{V^+}{V} & \mathbf{x} \in \Omega^- \end{cases} \quad (31)$$

Here the coordinate  $\xi$  has been expressed as a projection of a distance with respect to to the  $\Gamma_d$  plane and a domain-dependent scalar  $\Theta$  containing the volume ratios has been defined. It's important to note that the intent of this work to derive this already-known enhancement field shape is to demonstrate that, instead of starting with a seemingly arbitrary definition [29, 14], its final form comes rather from the application of a definite set of constraints. This sheds light on the theoretical basis on which this family of enhancements is built upon.

From Eq. 30, general expressions for the  $\mathbf{G}_w^\pm$  operators can be found on the global reference frame by applying the symmetrical gradient operator in global coordinates. Einstein index notation is useful to reach the following typical strain field tensor expression in terms of symmetric dyadic products:

$$\tilde{\boldsymbol{\varepsilon}} = \Theta \left[ [\varepsilon]_n (\mathbf{n} \otimes \hat{\mathbf{n}})^s + 2 [\varepsilon]_m (\mathbf{n} \otimes \hat{\mathbf{m}})^s + 2 [\varepsilon]_t (\mathbf{n} \otimes \hat{\mathbf{t}})^s \right], \quad (32)$$

where factors of 2 have been accounted for in the shear strain-related terms to ease the use of 3D constitutive laws. This expression is converted into a Voigt format to finally obtain:

$$\tilde{\boldsymbol{\varepsilon}} = \mathbf{G}_w^\pm [|\boldsymbol{\varepsilon}|] = \Theta \mathbf{H}_w [|\boldsymbol{\varepsilon}|], \quad \mathbf{H}_w = \begin{bmatrix} n_x^2 & n_x m_x & n_x t_x \\ n_y^2 & n_y m_y & n_y t_y \\ n_z^2 & n_z m_z & n_z t_z \\ n_x n_y + n_y n_x & n_x m_y + n_y m_x & n_x t_y + n_y t_x \\ n_z n_y + n_y n_z & n_z m_y + n_y m_z & n_z t_y + n_y t_z \\ n_z n_x + n_x n_z & n_z m_x + n_x m_z & n_z t_x + n_x t_z \end{bmatrix} \quad (33)$$

Note that the domain-dependent term in all these definitions stands as a single scalar  $\Theta$  taking the form of domain volume ratios.

#### 4.2. Consistent enhancement analysis

For the case of a more variationally consistent enhancement field considering requirement 3 (Eq. 11), it is more practical to start the analysis by expressing the enhancement as a piece-wise definition of two linear fields using classical linear interpolation functions:

$$\tilde{\mathbf{u}}^+ = \tilde{\mathbf{u}}_1^+ \phi_1 + \tilde{\mathbf{u}}_2^+ \phi_2 + \tilde{\mathbf{u}}_3^+ \phi_3 + \tilde{\mathbf{u}}_4^+ \phi_4 \quad (34a)$$

$$\tilde{\mathbf{u}}^- = \tilde{\mathbf{u}}_1^- \phi_1 + \tilde{\mathbf{u}}_2^- \phi_2 + \tilde{\mathbf{u}}_3^- \phi_3 + \tilde{\mathbf{u}}_4^- \phi_4 \quad (34b)$$

where the interpolation functions  $\phi$  associated each node  $i$  of a base linear tetrahedron have been defined as  $\phi_i = a_i + b_i \xi + c_i \eta + d_i \zeta$ , where all coefficients  $a_i, b_i, c_i, d_i$  are known. This time, the goal of the model particularisation is to find the value of all the nodal enhanced displacements  $\tilde{\mathbf{u}}_i^\pm$  as a function of nodal coordinate information and the weak discontinuity internal variables.

An auxiliary variable  $p_i$  is defined as a position indicator between the  $\Omega^+$  and the  $\Omega^-$  domains as follow:

$$p_i = \begin{cases} 1 & \mathbf{x}_i \in \Omega^+ \\ 0 & \mathbf{x}_i \in \Omega^- \end{cases} \quad i = \{1, 2, 3, 4\} \quad (35)$$

Using this variable, a general *mixed* velocity variable  $\tilde{\mathbf{u}}_i$  is defined:

$$\tilde{\mathbf{u}}_i = (1 - p_i) \tilde{\mathbf{u}}_i^+ + p_i \tilde{\mathbf{u}}_i^-, \quad i = \{1, 2, 3, 4\} \quad (36)$$

Having all that, we can start by the application of requirement 3 (Eq. 11) in a very straight-forward fashion by just nullifying some nodal enhanced displacements in their corresponding domains. This leads to:

$$\tilde{\mathbf{u}}^+ = \sum_i^N (1 - p_i) \tilde{\mathbf{u}}_i^+ \phi_i \quad (37a)$$

$$\tilde{\mathbf{u}}^- = \sum_i^N p_i \tilde{\mathbf{u}}_i^- \phi_i \quad (37b)$$

This also implies that the mixed variable  $\tilde{\mathbf{u}}_i$  actually *captures the set of all non-zero  $\tilde{\mathbf{u}}_i^\pm$  variables to be solved* for in this process.

Next, displacement continuity (requirement 1) is applied:

$$\tilde{\mathbf{u}}^+ \Big|_{\xi=0} = \tilde{\mathbf{u}}^- \Big|_{\xi=0} \quad (38a)$$

$$\sum_i^N (1 - p_i) \tilde{\mathbf{u}}_i^+ (a_i + c_i \eta + d_i \zeta) = \sum_i^N p_i \tilde{\mathbf{u}}_i^- (a_i + c_i \eta + d_i \zeta) \quad (38b)$$

where the mixed variable  $\tilde{\mathbf{u}}_i$  can be used to reach the following:

$$\sum_i^N (1 - 2p_i) a_i \tilde{\mathbf{u}}_i = 0 \quad \sum_i^N (1 - 2p_i) c_i \tilde{\mathbf{u}}_i = 0, \quad \sum_i^N (1 - 2p_i) d_i \tilde{\mathbf{u}}_i = 0 \quad (39)$$

The strain jump requirement 2 follows exactly the same process followed previously in Eqs. 25a-25d to find expressions relating enhanced nodal displacements to weak discontinuity internal variables:

$$\sum_i^N b_i \tilde{u}_{in} = [\varepsilon]_n \quad \sum_i^N b_i \tilde{u}_{it} = 2 [\varepsilon]_t, \quad \sum_i^N b_i \tilde{u}_{im} = 2 [\varepsilon]_m \quad (40)$$

where  $\tilde{u}_{in}, \tilde{u}_{it}, \tilde{u}_{im}$  are the three components of each non-zero  $\tilde{\mathbf{u}}_i$  on the local directions associated to each node  $i$ .

At this point, it's worth stopping to make a variable summary on the linear system being currently built for all non-zero enhanced nodal displacements  $\tilde{\mathbf{u}}_i$ . All non-zero variables corresponding to each direction  $\hat{\mathbf{n}}, \hat{\mathbf{t}}, \hat{\mathbf{m}}$  can be grouped in single vectors  $\tilde{\mathbf{u}}_n, \tilde{\mathbf{u}}_t, \tilde{\mathbf{u}}_m$  as follows:

$$\tilde{\mathbf{u}}_n = \begin{bmatrix} \tilde{u}_{1n} \\ \tilde{u}_{2n} \\ \tilde{u}_{3n} \\ \tilde{u}_{4n} \end{bmatrix}, \tilde{\mathbf{u}}_t = \begin{bmatrix} \tilde{u}_{1t} \\ \tilde{u}_{2t} \\ \tilde{u}_{3t} \\ \tilde{u}_{4t} \end{bmatrix}, \tilde{\mathbf{u}}_m = \begin{bmatrix} \tilde{u}_{1m} \\ \tilde{u}_{2m} \\ \tilde{u}_{3m} \\ \tilde{u}_{4m} \end{bmatrix} \quad (41)$$

The system can then be summarized using block matrix definitions:

$$\begin{bmatrix} \mathbf{C}_e & \mathbf{0}_4 & \mathbf{0}_4 \\ \mathbf{0}_4 & \mathbf{C}_e & \mathbf{0}_4 \\ \mathbf{0}_4 & \mathbf{0}_4 & \mathbf{C}_e \end{bmatrix} \begin{bmatrix} \tilde{\mathbf{u}}_n \\ \tilde{\mathbf{u}}_t \\ \tilde{\mathbf{u}}_m \end{bmatrix} = \begin{bmatrix} [\varepsilon]_{n,e} \\ [\varepsilon]_{m,e} \\ [\varepsilon]_{t,e} \end{bmatrix}, \quad (42)$$

where:

$$\mathbf{C}_e = \begin{bmatrix} (1 - 2p_1) a_1 & (1 - 2p_2) a_2 & (1 - 2p_3) a_3 & (1 - 2p_4) a_4 \\ (1 - 2p_1) b_1 & (1 - 2p_2) b_2 & (1 - 2p_3) b_3 & (1 - 2p_4) b_4 \\ (1 - 2p_1) c_1 & (1 - 2p_2) c_2 & (1 - 2p_3) c_3 & (1 - 2p_4) c_4 \\ (1 - 2p_1) d_1 & (1 - 2p_2) d_2 & (1 - 2p_3) d_3 & (1 - 2p_4) d_4 \end{bmatrix}, \mathbf{0}_4 = \begin{bmatrix} 0 & 0 & 0 & 0 \\ 0 & 0 & 0 & 0 \\ 0 & 0 & 0 & 0 \\ 0 & 0 & 0 & 0 \end{bmatrix} \quad (43a)$$

$$[\varepsilon]_{n,e} = \begin{bmatrix} 0 \\ [\varepsilon]_n \\ 0 \\ 0 \end{bmatrix}, \quad [\varepsilon]_{t,e} = 2 \begin{bmatrix} 0 \\ [\varepsilon]_t \\ 0 \\ 0 \end{bmatrix}, \quad [\varepsilon]_{m,e} = 2 \begin{bmatrix} 0 \\ [\varepsilon]_m \\ 0 \\ 0 \end{bmatrix} \quad (43b)$$

The system already counts with 12 enhanced nodal displacement variables and 12 equations, which render it closed with a unique solution if the coefficient matrix in Eq. 42 is not singular. Further application of requirement 4 (the patch test) *does not* add any new variables to the system. Therefore, it can be stated that for a linear definition of the enhanced field  $\tilde{\mathbf{u}}$ , it is **not possible** to make a variationally symmetric definition for the  $\mathbf{G}_w$  matrix operators having a unique base enhanced displacement field. To be fully consistent while keeping linear definitions, the framework requires to make  $\mathbf{G}_w \neq \mathbf{G}_w^*$ , taking requirement 4 (Eq. 19) as

the guidance to define  $\mathbf{G}_w^*$  and the other requirements to define  $\mathbf{G}_w$  in a separate way. The typical weak discontinuity enhanced field (Eq. 30.) thus cannot be, by definition, variationally consistent.

The analysis on this section will continue to particularize the enhanced field with the system proposed in Eq. 42. As the system is block-diagonal, a compact-closed solution is found:

$$\tilde{\mathbf{u}}_n = \begin{bmatrix} C_{1,2}^{-1} \\ C_{2,2}^{-1} \\ C_{3,2}^{-1} \\ C_{4,2}^{-1} \end{bmatrix} [\varepsilon]_n, \quad \tilde{\mathbf{u}}_t = 2 \begin{bmatrix} C_{1,2}^{-1} \\ C_{2,2}^{-1} \\ C_{3,2}^{-1} \\ C_{4,2}^{-1} \end{bmatrix} [\varepsilon]_t, \quad \tilde{\mathbf{u}}_m = 2 \begin{bmatrix} C_{1,2}^{-1} \\ C_{2,2}^{-1} \\ C_{3,2}^{-1} \\ C_{4,2}^{-1} \end{bmatrix} [\varepsilon]_m, \quad (44)$$

where the  $C_{i,2}^{-1}$  coefficients come from the second column of the inverse of the  $\mathbf{C}_e$  matrix. The particularized enhanced field can then be expressed as:

$$\tilde{\mathbf{u}}^+ = \sum_i^{N_e} (1 - p_i) C_{i,2}^{-1} \phi_i \begin{bmatrix} [\varepsilon]_n \\ 2 [\varepsilon]_t \\ 2 [\varepsilon]_m \end{bmatrix}, \quad \tilde{\mathbf{u}}^- = \sum_i^{N_e} p_i C_{i,2}^{-1} \phi_i \begin{bmatrix} [\varepsilon]_n \\ 2 [\varepsilon]_t \\ 2 [\varepsilon]_m \end{bmatrix} \quad (45)$$

Finally, the consistent weak enhancement field can still be written in the familiar format:

**Weak discontinuity enhancement: consistent definition**

$$\tilde{\mathbf{u}} = \Theta \left( [\varepsilon]_n \hat{\mathbf{n}} + 2 [\varepsilon]_t \hat{\mathbf{m}} + 2 [\varepsilon]_m \hat{\mathbf{t}} \right) \quad (46)$$

$$\Theta = \begin{cases} \Theta^+ = \sum_i^{N_e} (1 - p_i) C_{i,2}^{-1} \phi_i & x \in \Omega^+ \\ \Theta^- = \sum_i^{N_e} p_i C_{i,2}^{-1} \phi_i & x \in \Omega^- \end{cases} \quad (47)$$

It's important to note that, while  $\Theta$  stays as a constant in the typical enhancement model, it becomes a variable parameter on the consistent model depending on nodal coordinates embedded in the interpolation functions  $\phi_i$ .

The  $\mathbf{G}_w^\pm$  operators can be devised again by making use of the symmetric gradient operator. Taking, for instance, the enhanced strain field on the  $\Omega^+$  domain one can reach an analogous tensor expression to that of the typical model:

$$\tilde{\boldsymbol{\varepsilon}}^+ = \sum_i^{N_e} (1 - p_i) C_{i,2}^{-1} \left[ [\varepsilon]_n (\mathbf{e}_i \otimes \hat{\mathbf{n}})^s + 2 [\varepsilon]_t (\mathbf{e}_i \otimes \hat{\mathbf{m}})^s + 2 [\varepsilon]_m (\mathbf{e}_i \otimes \hat{\mathbf{t}})^s \right] \quad (48a)$$

$$\mathbf{e}_i = [b_i \quad c_i \quad d_i]^T \quad (48b)$$

Here, the vector  $\mathbf{e}_i$  coming from *local* interpolation function coefficients, has to be transformed (rotated) to global coordinates as needed. Again, expressing in a Voigt vector field format:

$$\tilde{\boldsymbol{\varepsilon}}^+ = \mathbf{G}_w^+ [[\varepsilon]] = \sum_i^{N_e} (1 - p_i) C_{i,2}^{-1} \mathbf{H}_{W,i} [[\varepsilon]] \quad (49a)$$

$$\mathbf{H}_{W,i} = \begin{bmatrix} b_i n_x & b_i m_x & b_i t_x \\ c_i n_y & c_i m_y & c_i t_y \\ d_i n_z & d_i m_z & d_i t_z \\ b_i n_y + c_i n_x & b_i m_y + c_i m_x & b_i t_y + c_i t_x \\ d_i n_y + c_i n_z & d_i m_y + c_i m_z & d_i t_y + c_i t_z \\ d_i n_x + b_i n_z & d_i m_x + b_i m_z & d_i t_x + b_i t_z \end{bmatrix} \quad (49b)$$

where the coefficients  $b_i, c_i, d_i$  are already taken from a rotated  $\mathbf{e}_i$  vector in this global definition.  $\mathbf{G}_w^-$  follows in a similar way:

$$\tilde{\boldsymbol{\varepsilon}}^- = \mathbf{G}_w^- [|\boldsymbol{\varepsilon}|] = p_i C_{i,2}^{-1} \mathbf{H}_{W,i} [|\boldsymbol{\varepsilon}|] \quad (50)$$

The virtual operators  $\mathbf{G}_w^{*\pm}$  only have the goal of complying with the patch test (requirement 4). If the simplest, constant definition for them is adopted, satisfaction of Eq. 20 allows an infinite amount of choices.  $\mathbf{G}_w^{*\pm}$  can even take the form of the typical enhancement (Eq. 33), which has been already built to satisfy Eq. 20.

#### 4.3. A discussion on enhancement stability properties

The stability of the weak discontinuity model can be assessed by observing that in Eq. 21e, the calculation of the weak discontinuity variables  $[\boldsymbol{\varepsilon}]_t, [\boldsymbol{\varepsilon}]_t, [\boldsymbol{\varepsilon}]_m$  as a function of nodal standard displacements  $\mathbf{d}$  depends on the inverse of a  $\mathbf{K}_{ww}$  stiffness matrix. The behavior of  $\mathbf{K}_{ww}$ , depending on the form of the enhancement operators, will determine if the formulation becomes unstable under certain conditions. No other mathematical stability sources are identified.

For a more direct analysis, it is convenient to work in the local frame  $(\hat{\mathbf{n}}, \hat{\mathbf{t}}, \hat{\mathbf{m}})$ . It will be assumed that the consistent enhancement will use the same operators  $\mathbf{G}_w^{*\pm}$  as the typical enhancement, while retaining the real operators  $\mathbf{G}_w^\pm$  as devised in Section 4.2. If this is the case, both formulations will share the same  $\mathbf{H}_w$  operator for virtual fields, which in local coordinates reduces to:

$$\mathbf{H}_w^T = \begin{bmatrix} 1 & 0 & 0 & 0 & 0 & 0 \\ 0 & 0 & 0 & 1 & 0 & 0 \\ 0 & 0 & 0 & 0 & 0 & 1 \end{bmatrix} \quad (51)$$

For a typical weak discontinuity enhancement, Eq. 21d can be developed to get to the following:

$$\mathbf{K}_{ww} = \frac{V^+ V^-}{V^2} \mathbf{H}_w^T (\mathbf{C}^+ V^- + \mathbf{C}^- V^+) \mathbf{H}_w, \quad (52)$$

where linear elastic constitutive matrices in three dimensions can be assumed for the corresponding materials on  $\Omega^+$  and  $\Omega^-$  as:

$$\mathbf{C}^+ = \begin{bmatrix} c_1^+ & c_2^+ & c_2^+ & 0 & 0 & 0 \\ c_2^+ & c_1^+ & c_2^+ & 0 & 0 & 0 \\ c_2^+ & c_2^+ & c_1^+ & 0 & 0 & 0 \\ 0 & 0 & 0 & c_s^+ & 0 & 0 \\ 0 & 0 & 0 & 0 & c_s^+ & 0 \\ 0 & 0 & 0 & 0 & 0 & c_s^+ \end{bmatrix}, \mathbf{C}^- = \begin{bmatrix} c_1^- & c_2^- & c_2^- & 0 & 0 & 0 \\ c_2^- & c_1^- & c_2^- & 0 & 0 & 0 \\ c_2^- & c_2^- & c_1^- & 0 & 0 & 0 \\ 0 & 0 & 0 & c_s^- & 0 & 0 \\ 0 & 0 & 0 & 0 & c_s^- & 0 \\ 0 & 0 & 0 & 0 & 0 & c_s^- \end{bmatrix} \quad (53)$$

for some real, positive constants  $c_1^\pm, c_2^\pm, c_s^\pm$ . Taking these definitions, the  $\mathbf{K}_{ww}$  matrix associated to the typical enhancement can be calculated in a diagonal, compact expression:

$$\mathbf{K}_{ww} = \begin{bmatrix} V^+ c_1^+ + V^- c_1^- & 0 & 0 \\ 0 & V^+ c_s^+ + V^- c_s^- & 0 \\ 0 & 0 & V^+ c_s^+ + V^- c_s^- \end{bmatrix} \quad (54)$$

As the constants  $c_1^\pm, c_s^\pm$  stay real and positive as well as the subvolumes  $V^+, V^-$ , Eq. 54 reveals that the typical weak discontinuity enhancement turns out to be **unconditionally stable**, no matter what the orientation of the interface, the subvolume partition and the material elasticity characteristics are. This is one of the most prominent reasons why, despite not being variationally consistent by definition, authors in [14, 30, 31] have been keen to keep it on their heterogeneity modelling approaches, as it eases the implementation process and the numerical solution control.

Working with the consistent enhancement, Eq. 21d returns the following expression:

$$\mathbf{K}_{ww} = \frac{V^+V^-}{V} \mathbf{H}_w^T \sum_i^{N_e} C_{i,2}^{-1} [(1-p_i) \mathbf{C}^+ - p_i \mathbf{C}^-] \mathbf{H}_{w,i}, \quad (55)$$

where the node-dependant matrix  $\mathbf{H}_{wi}$  can be reduced to:

$$\mathbf{H}_{wi}^T = \begin{bmatrix} b_i & 0 & 0 & c_i & 0 & d_i \\ 0 & c_i & 0 & b_i & d_i & 0 \\ 0 & 0 & d_i & 0 & c_i & b_i \end{bmatrix} \quad (56)$$

Taking the same constitutive matrix definitions in Eq. 53, the  $\mathbf{K}_{ww}$  for this case can be devised as:

$$\mathbf{K}_{ww} = \frac{V^+V^-}{V} \sum_i^{N_e} C_{i,2}^{-1} \begin{bmatrix} b_i k_{1i} & c_i k_{2i} & d_i k_{2i} \\ c_i k_{si} & b_i k_{si} & 0 \\ d_i k_{si} & 0 & b_i k_{si} \end{bmatrix} \quad (57)$$

where the  $k_{ji}$  parameters are defined as follows:

$$k_{1i} = (1 - 2p_i) c_1^{(1-2p_i)} \quad (58a)$$

$$k_{1i} = (1 - 2p_i) c_2^{(1-2p_i)} \quad (58b)$$

$$k_{1i} = (1 - 2p_i) c_s^{(1-2p_i)} \quad (58c)$$

The structure of Eq. 57 is considerably more complex than that of Eq. 54, where in the former we can appreciate a more extensive participation of elemental parameters such as interpolation function coefficients and functions that are domain dependent (interface location/orientation dependent) within nodal summations. No unconditional stability can be readily assured in Eq. 57.

While the specific subspace of parameters that drive  $\mathbf{K}_{ww}$  unstable for the consistent enhancement will not be calculated in a rigorous fashion on this work, it is not hard to see that there's a condition that will intuitively introduce mathematical ambiguity problems: when the interface plane crosses exactly or very close to one or more element nodes, where it makes a sudden change of behaviour. If a given finite element model manages a non-structured mesh with random orientations while also having random material interfaces, instability or near-instability conditions will be certain to happen in some elements with a sufficiently large mesh. Implementation efforts have to consider this fact.

#### 4.4. Stiffness matrices and impact the to global solution process

One of the most attractive features of the E-FEM framework is the ability to limit the work with field enhancements and all their associated variables within internal element calculation routines. All stiffness calculations derived from the special internal calculations associated to the discontinuities can be condensed and integrated to the standard elemental stiffness matrix. This way, no formal degrees of freedom are added to the finite element global solution process, so that the methods, routines and the solution platform shall remain untouched. However, the classical stiffness matrix properties normally identified in standard finite elements may change depending on the structure of the embedded enhancement.

For the weak discontinuity enhancements presented in this work, the numerical solution process and the construction of an *equivalent* stiffness matrix can be started by taking Eq. 7a (elemental force balance) and Eq. 21b (main relation between nodal displacements and weak discontinuity variables) to build the following linear system:

$$\mathbf{K}_{bb} \mathbf{d} + \mathbf{K}_{bw} [|\boldsymbol{\varepsilon}|] = \mathbf{f}_{ext}^e \quad (59a)$$

$$\mathbf{K}_{wb} \mathbf{d} + \mathbf{K}_{ww} [|\boldsymbol{\varepsilon}|] = \mathbf{0} \quad (59b)$$

Here, Eq. 7a has been integrated using the previously defined operators depending on the enhancement version to define stiffness matrices  $\mathbf{K}_{bb}$  and  $\mathbf{K}_{bw}$ .

Condensation of the system then takes place by reducing  $[\boldsymbol{\varepsilon}]$  from Eq. 59b and substituting on Eq. 59a, giving rise to a definition of an equivalent elemental stiffness matrix  $\mathbf{K}_{sc}$  multiplying the standard normal displacements vector  $\mathbf{d}$ :

$$\mathbf{K}_{sc}\mathbf{d} = \mathbf{f}_{ext}^e \quad (60a)$$

$$\mathbf{K}_{sc} = \mathbf{K}_{bb} - \mathbf{K}_{bw}\mathbf{K}_{ww}^{-1}\mathbf{K}_{wb} \quad (60b)$$

With this, a global stiffness matrix assembly process may then be performed by taking the corresponding matrices  $\mathbf{K}_{sc}$  associated to each element on a given model.

For the case of a typical weak discontinuity enhancement, it is not hard to see that:

$$\mathbf{K}_{bw} = \frac{V^+V^-}{V}\mathbf{B}^T [\mathbf{C}^+ - \mathbf{C}^-] \mathbf{H}_w = \left\{ \frac{V^+V^-}{V}\mathbf{H}_w^T [\mathbf{C}^+ - \mathbf{C}^-] \mathbf{B} \right\}^T = \mathbf{K}_{wb}^T \quad (61)$$

so that:

$$(\mathbf{K}_{bw}\mathbf{K}_{ww}^{-1}\mathbf{K}_{wb})^T = \mathbf{K}_{wb}^T\mathbf{K}_{ww}^{-T}\mathbf{K}_{bw}^T = \mathbf{K}_{bw}\mathbf{K}_{ww}^{-1}\mathbf{K}_{wb} \quad (62)$$

Given that  $\mathbf{K}_{bb}$  is already symmetric, it can be concluded that the condensation process will always return a **symmetric**  $\mathbf{K}_{sc}$ . On the other hand, with the consistent enhancement, this is not the case:

$$\left\{ \mathbf{B}^T \sum_i^{N_e} C_{i,2}^{-1} [(1-p_i)V^+ + p_iV^-] \mathbf{C}\mathbf{H}_{w,i} \right\}^T \neq \frac{V^+V^-}{V}\mathbf{H}_w^T [\mathbf{C}^+ - \mathbf{C}^-] \mathbf{B} \quad (63a)$$

$$\mathbf{K}_{bw} \neq \mathbf{K}_{wb}^T \quad (63b)$$

This is, the consistent enhancement will, *in general*, return an **asymmetrical** stiffness matrix. This will introduce the need to use asymmetric solvers during a global numerical solution, with all computational and implementation implications that come along. This could be already perceived from the variational formulation itself, where the typical enhancement always managed the same operators for both virtual and real fields while the consistent enhancement didn't.

#### 4.5. Variational consistency errors in the typical enhancement

Now that it is known that the typical enhancement in general will not comply with basic requirement 3 (Eq. 11), it is relevant to discuss the conditions under which the formulation might produce large variational errors and the ones in which these errors will be kept within a reasonable range.

For a case of a 1-D element, like in the applications done by Benkemoun [38] or Melnyk [26], there can be only one node on each side of the material interface, and its orientation will always be normal to the line defining the body of the element. Under these conditions, it can be shown that the only difference between a typical and a consistent enhancement is only a constant offset  $\Delta\tilde{u}$  on the displacement function (refer to Fig. 3). Given that the slopes coincide and the operators of the formulation are based on field derivatives, it can be concluded that the typical formulation effectively complies with requirement 3 and thus also remains fully variationally consistent.

For 2D and 3D elements in general, this is not the case. The slope of the typical enhancement will always be aligned to the orientation of the interface  $\Gamma_d$ . If more than one node is present on one of the domains, the enhancement will not be able to return the same field value on all nodes simultaneously, no matter what offset is given to the field. The only condition in which this might happen is when the nodes within

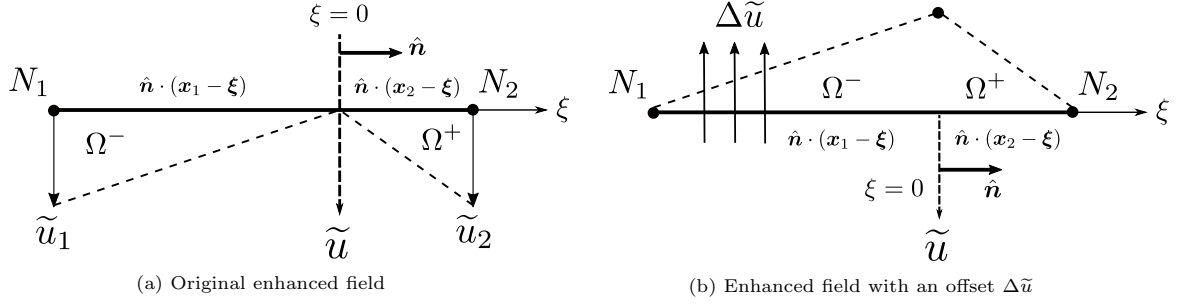


Figure 3: Graphical analysis on 1D typical weak discontinuity enhancements. Nullification of the field at element nodes can be achieved by adding an offset  $\Delta \tilde{u}$

a domain are all located on the same  $\xi$  coordinate, which would mean having element geometry aligned to the material interface. As the respective nodal  $\xi$  coordinates start to divert, the typical field will miss to opportunity to nullify the values at the boundaries. Figure 4 illustrates this for a 2D constant stress triangle (CST). The offset  $\Delta \tilde{u}$  can be arranged to minimize this variational error by making the field to roughly pass through zero at an *average*  $\xi$  position of all nodes on a given domain.

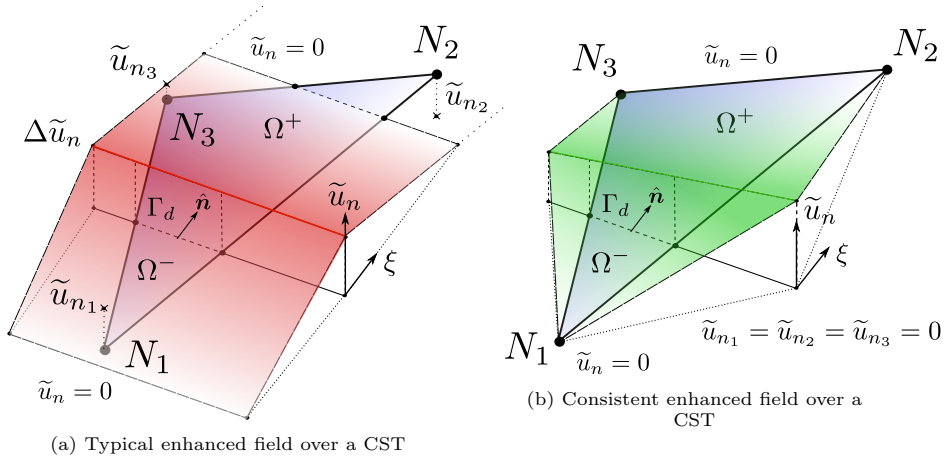


Figure 4: Graphical analysis on 2D typical weak discontinuity enhancements taking a constant stress triangle (CST) as the base element, compared to a consistent enhancement. For the typical enhancement, it is assumed that an offset  $\Delta \tilde{u}_n$  has been given to the field to minimize the error when trying to nullify field values on the CST nodes.

Based on this rationale, the typical enhancement can be perceived as an *average estimation* of a fully consistent enhancement that will be closer to it under certain mesh geometry conditions. It can be expected that for an unstructured mesh with good aspect ratios, this estimation will grant reasonable results compared to a fully consistent approach. For a heavily distorted mesh having a very large disparity on  $\xi$  coordinates within a domain, the variational errors induced will certainly get larger.

## 5. Numerical simulations

In this section, a numerical comparison takes place between both weak discontinuity enhancements to discuss their performance with respect to an analytical solution to a given problem.

### 5.1. Numerical model description

Numerical simulations have been done on a simple cube model made up of two material layers separated by a planar interface. The interface is parallel to two of the cube faces. If interface concentrations are

neglected, the total axial reaction associated to a normal displacement on one of the faces can be calculated by means of the classical theory of mechanics of materials, representing the system as two springs in series accounting for the axial stiffness of each layer. Linear elastic behavior is assumed for both materials, characterized by Young Moduli  $E^+$ ,  $E^-$  and Poisson ratios  $\nu^+$ ,  $\nu^-$ . Figure 5 illustrates this simple mechanical system.

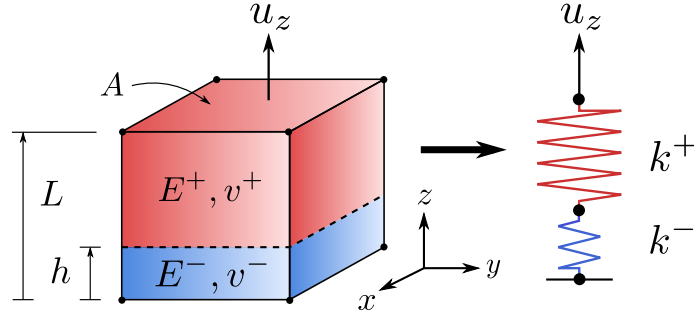


Figure 5: Basic description of a bi-material layered prismatic body with total height  $L$  and cross section  $A$ , treated as a two-spring mechanical system in series having constants  $k^+$  and  $k^-$ . The stiffness partition depends of the position  $h$  of the interface plane.

The idea of the present study is to compare how each of the weak discontinuity enhancements can model this ideal bi-material layout by comparing to the classical analytical solution. The interface plane location  $h$  will be varied taking regular steps from having a zero position at one of the cube faces until reaching the opposite side of the cube. This will represent situations in which the cube starts completely homogeneous with one of the material phases and gradually becomes entirely filled with the other material phase.

The cube will feature an unstructured mesh, totally independent from the planar interface. The interface will cross a certain amount of elements on random edges and positions, and these elements will be enhanced with one of the weak discontinuity field functions studied in previous sections. Special care has been taken with the mesh density: the size of the elements should be small enough to generate enough enhanced elements, but these special elements should cover a significant amount of cube volume in order for them to really have a meaningful contribution to the global response of the model. Otherwise, if the elements are too small, we might effectively get a large number of enhanced elements near the interface, but also a much larger amount of *normal* elements having completely one material phase or the other, and thus the global stiffness response of the numerical sample will be dominated by the standard finite elements instead, which are not the object of this study. The mesh finally selected for this study is shown in Figure 6, also highlighting the number of enhanced elements resulting from having the planar interface at 30% height from the designed bottom position. It's pertinent to mention that the quality of the mesh has been kept rather high, with no aspect ratios going beyond 3.

The cube has dimensions of  $10\text{ mm} \times 10\text{ mm} \times 10\text{ mm}$ . The material properties chosen for these simulations have been those normally associated to a simplified concrete mixture: a material phase of mortar (Young modulus  $E^- = 14000\text{ MPa}$ , Poisson ratio  $\nu^- = 0.2$ ) and an aggregate material ( $E^+ = 70000\text{ MPa}$ ,  $\nu^+ = 0.2$ ). No other material properties are needed since all simulations will be made in static conditions. Boundary conditions have been set as to retain an ideal axial prism problem as much as possible without significant effects of near-interface field concentrations. The load has been imposed as a uniform displacement of  $0.015\text{ mm}$  on the free upper face. Figure 7 illustrates the details of the model.

FEAP (Finite Element Analysis Program) (REF) has been used as the finite element numerical solution platform to implement both enhancements described in previous sections and for simulating the problem mentioned beforehand. 21 static-implicit simulations have been performed considering each weak discontinuity enhancement approach having 21 uniformly separated positions for the interface plane, going from the lower  $z$  face of the cube ( $h = 0$ ) all the way to the opposite face ( $h = 10\text{ mm}$ ) taking steps of  $0.5\text{ mm}$ . The

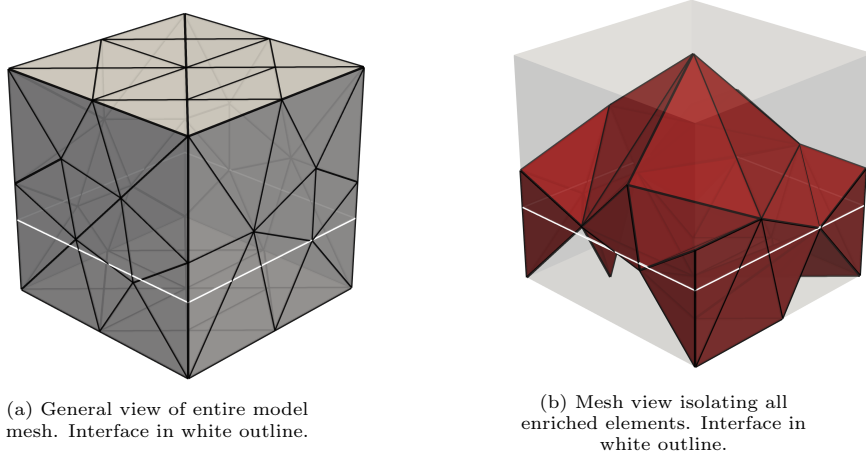


Figure 6: General mesh description and a view of all enriched elements crossed by the material interface plane. 92 elements and 43 nodes are used for the entire model. Enriched elements make up approximately for 50% of total volume.

solution is strictly linear elastic, where the only solver-specific difference between each enhancement case has been the use of symmetric and asymmetric stiffness matrix handling routines, which are used only one time at the beginning of each analysis. Direct linear equation system solvers are used in either case.

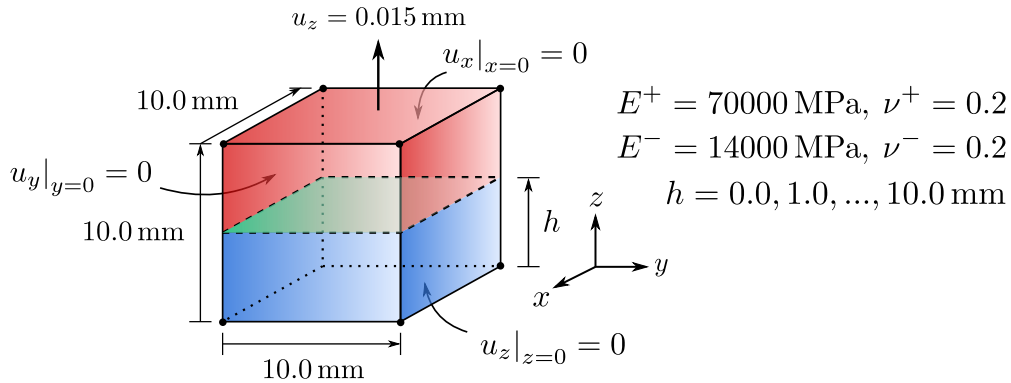


Figure 7: Description of model details, as simulated in the FEAP program.

## 5.2. Results and discussion

Two different kinds of results have been considered for the current discussion in this work. One is the total vertical force reaction associated to the imposed displacement load for each case of interface plane position. The analytical calculation can be easily done attending to the representation in Figure 5 and finding the total vertical reaction through an equivalent stiffness  $k_{eq}$ :

$$F_z = u_z k_{eq} \quad (64a)$$

$$k_{eq} = \frac{k^+ k^-}{k^+ + k^-} \quad (64b)$$

$$k^\pm = \frac{SE^\pm}{L^\pm} \quad (64c)$$

The other output of interest is the average strain field value on each side of the interface. Analytically, these values are easily obtainable by just making:

$$\varepsilon^\pm = \frac{\sigma^\pm}{E^\pm} = \frac{F_{eq}}{SE^\pm} \quad (65)$$

Numerical simulation results coming from both enhancement types for the vertical force reaction can be appreciated in Figure 8. The first and last points in this plot represent the cases in which homogeneous material distributions are given for one or the other material phases (stiffer case and more compliant case, respectively), in which all numerical and analytical models naturally coincide. In the first part of the curves where the stiffer material is predominant, both weak discontinuity enhancements coincide for a while having a consistent error with respect to the analytical curve. At some point after having at least 20% volume fraction of the (-) material region, the consistent enhancement error drops almost entirely, closely sticking to the analytical curve until the end of the graph. The typical enhancement maintains a smooth behavior with a consistent error, which also fades at the end when the (-) material dominates completely. A maximum error of approximately 14% is observed with the typical enhancement. The sudden variations on the consistent enhancement can be explained by its natural stability conditions depending on node positions relative to the cutting plane interface, already discussed in Section 4.3.

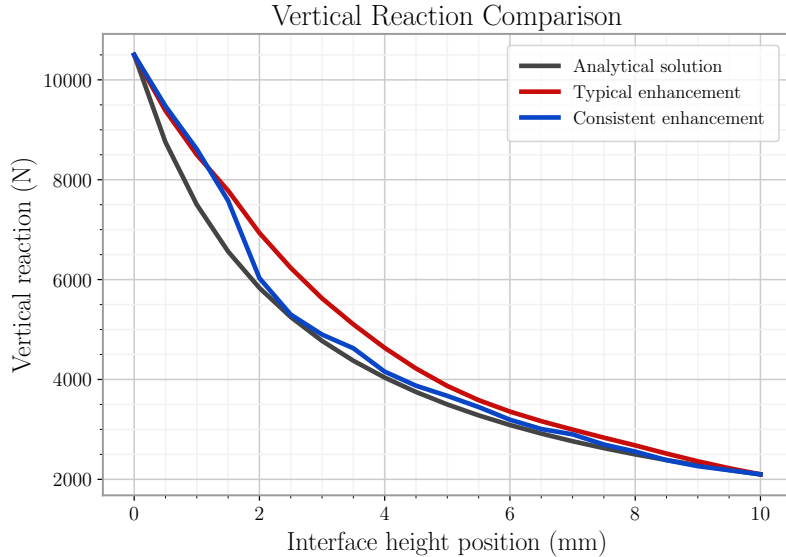


Figure 8: Vertical reaction on the entire lower face of the cube model for both enhancement types and the analytical solution.

The displacement load imposed to this simple model will ideally produce a piece-wise, constant strain field. The numerical approaches should be able to produce these constant strain regions taking the contribution of all elements on each side of the interface, aiming to have the least dispersion as possible. For this, the *average* strain field and its *dispersion* (standard deviation) have been calculated on each side of the cube model interface for both enhancement approaches, and results have been compared to the analytical model. The analytical results, of course, do not show any kind of field dispersion as they only exhibit a unique strain value. Figure 9 shows this comparison for the case of the (+) material side. Again, at homogeneous conditions all models coincide. Both enhancements start diverging at the beginning and the consistent enhancement quickly catches up the analytical behavior with a mild error. The typical enhancement, once again, has a smoother curve keeping a sustained error. The last data point at  $h = 10$  mm is not shown since the (+) region ceases to exist. The strain dispersion, represented as a translucent cloud around each enhancement curve, seems definitely more controlled for the consistent enhancement, albeit with apparently more erratic fluctuations coming from the stability nature of this formulation.

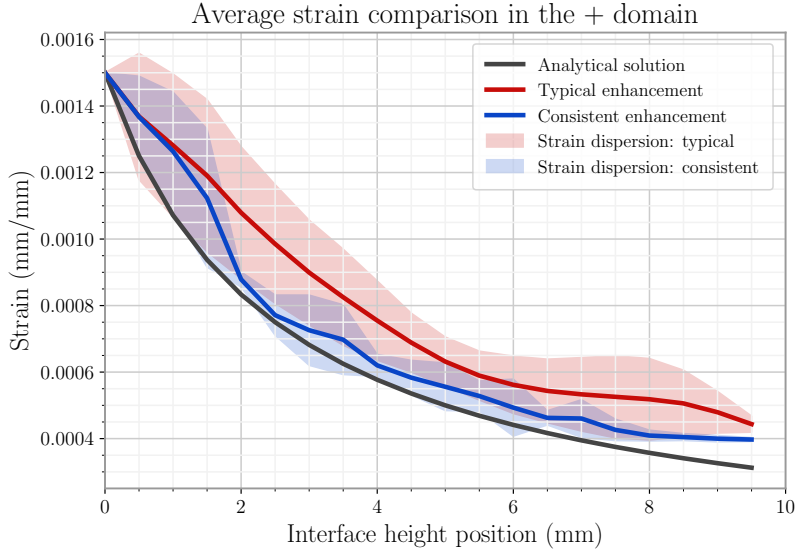


Figure 9: Average strain and corresponding dispersion for both weak discontinuity enhancements compared to analytical calculations on the (+) (stiffer material) domain.

Figure 10 shows the analysis on the remaining material region. In this case, it is the first point at zero that is missing since there is no (−) material. The average strain again favours the consistent enhancement that keeps a lower error through all conditions. The dispersion of the consistent model is also remarkably low, with the exception of one point at 30% volume for the (−) material, where an outlier data point occurs. After model inspections, it is indeed found that at this height many nodes lie very close to the interface with separations as low as 0.03 mm, which seemingly compromise the stability of this enhancement as discussed in section 4.3. The impact of this outlier is not noticeable for the case of the analysis on the (+) domain, since at  $h = 3$  mm there are considerably more homogeneous elements made up of the (+) material, which help to smooth these statistics.

## 6. Conclusions

A detailed analysis has been made on the use of weak discontinuity approaches within the E-FEM framework to model material heterogeneities. Kinematic and variational foundations have been stated to identify a set of consistency requirements for the general construction of weak discontinuity displacement enhancement fields. Based on the consideration of these requirements, two field proposals have been derived: one which has been already used in the works of [14, 35, 31] and other which is fully consistent with all requirements.

Simulations have been made on a simple bi-material system subject to an axial load to assess the performance of the enhancements. It has been seen that, in general, the consistent enhancement has a better performance than the typical enhancement at representing the expected response, but is more prone to uncontrolled fluctuations. It can be also argued, however, that under high quality mesh conditions and moderate difference between the elastic properties of material phases (a ratio of 5 explored in this work), the typical field will have a reasonable behavior that will allow for sound estimations at local and global level mechanical outputs. The formulation by itself naturally presents unconditional stability and retains the symmetry of global stiffness matrices. The internal calculations required to particularise the function parameters are also considerably simpler than in the case of the consistent enhancement version. For these reasons, the authors of this study recommend its use whenever possible, especially when dealing with large

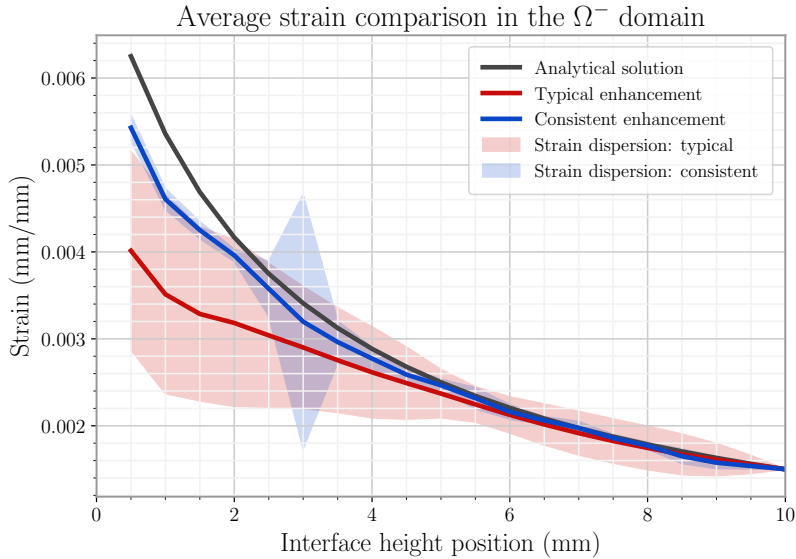


Figure 10: Average strain and corresponding dispersion for both weak discontinuity enhancements compared to analytical calculations on the  $(-)$  (more compliant) domain.

and complex numerical models where solution times and stability are crucial for the success of the numerical analysis project.

The use of the consistent weak discontinuity enhancement may find a better niche on problems where high accuracy is required for field shape calculations and where the use of an asymmetric solver poses no problem for a given FEM numerical solution platform. The authors in this work have found that the stability nuisances on the consistent formulation can actually be avoided at a large extent by just locally displacing the interface location slightly away from its compromising position, in such a way that the elemental volume distribution is just mildly changed without significantly affecting the physical representation aimed by the element in question.

The performance of the models has not been tested for badly shaped elements, where it is expected to have a worse behavior for the typical enhancement. Both enhancements also tend to have a slightly worse performance for locally describing stiffer materials within a bi-material set. It would also be relevant to study material sets with more prominent differences in elastic properties to assess the enhancements' behavior.

It can also be shown that a higher polynomial degree proposal for the weak discontinuity enhancement will be able to fulfill **all** consistency requirements *at once*. The study of its particular shape and properties could be an interesting topic for future work. This would allow an enhancement function both as robust as the typical and as accurate as the consistent one.

In either case, the authors of this work finish by stating that the use of weak discontinuity enhancements for the representation of material heterogeneities remains a reliable and efficient numerical method for approaching the problem of multiple material phases representation featuring non-adapted meshes.

## References

- [1] Y. Rémond, S. Ahzi, M. Baniassadi, H. Garmestani, Homogenization of Reconstructed RVE, John Wiley & Sons, Ltd, 2016, pp. 133–168. doi:<https://doi.org/10.1002/9781119307563.ch6>.
- [2] E. Weinan, Principles of Multiscale Modeling, Cambridge University Press, Cambridge, 2011.

- [3] Y. You, X. Kou, S. Tan, Adaptive meshing for finite element analysis of heterogeneous materials, *Computer-Aided Design* 62 (2015) 176–189.
- [4] M. Favino, J. Hunziker, E. Caspari, B. Quintal, K. Holliger, R. Krause, Fully-automated adaptive mesh refinement for media embedding complex heterogeneities: application to poroelastic fluid pressure diffusion, *Computational Geosciences* 24 (2020).
- [5] Y. Efendiev, C. Kronsbein, F. Legoll, Multilevel Monte Carlo approaches for numerical homogenization, *Multiscale Modeling and Simulation: A SIAM Interdisciplinary Journal* 13 (2015) 1107–1135.
- [6] M. Nikolic, E. Karavelić, A. Ibrahimbegovic, P. Mišević, Lattice element models and their peculiarities, *Archives of Computational Methods in Engineering* 25 (2018) 753–784.
- [7] T. Xu, T.-F. Fu, M. Heap, P. Meredith, T. Mitchell, P. Baud, Mesoscopic damage and fracturing of heterogeneous brittle rocks based on three-dimensional polycrystalline discrete element method, *Rock Mechanics and Rock Engineering* 53 (2020).
- [8] W. Shiu, F.-V. Donze, L. Daudeville, Compaction process in concrete during missile impact: a DEM analysis, *Computers and Concrete, an International Journal* 5 (2008) 329–342.
- [9] J. Huang, M. Chen, J. Sun, Mesoscopic characterization and modeling of microcracking in cementitious materials by the extended finite element method, *Theoretical and Applied Mechanics Letters* 4 (2014) 041001.
- [10] B. Vandoren, K. De Proft, A. Simone, L. Sluys, Mesoscopic modelling of masonry using weak and strong discontinuities, *Computer Methods in Applied Mechanics and Engineering* 255 (2013) 167–182.
- [11] G. Diwan, M. S. Mohamed, M. Seaid, J. Trevelyan, O. Laghrouche, Mixed enrichment for the finite element method in heterogeneous media, *International Journal for Numerical Methods in Engineering* (2015).
- [12] A. Moradi, S. Nazari, Computational modeling of strong and weak discontinuities using extended finite element method, *Mechanics of Advanced Materials and Structures* 23 (2015).
- [13] Y. Peng, X. Chen, L. Ying, Y. Chen, L. Zhang, Mesoscopic numerical simulation of fracture process and failure mechanism of concrete based on convex aggregate model, *Advances in Materials Science and Engineering* 2019 (2019) 1–17.
- [14] E. Roubin, A. Vallade, N. Benkemoun, J.-B. Colliat, Multi-scale failure of heterogeneous materials: A double kinematics enhancement for embedded finite element method, *International Journal of Solids and Structures* 52 (2015) 180 – 196.
- [15] M. Ortiz, Y. Leroy, A. Needleman, A finite element method for localized failure analysis, *Computer Methods in Applied Mechanics and Engineering* 61 (1987) 189–214.
- [16] T. Belytschko, J. Fish, B. E. Engelmann, A finite element with embedded localization zones, *Computer Methods in Applied Mechanics and Engineering* 70 (1988) 59–89.
- [17] L. Sluys, A. Berends, Discontinuous failure analysis for mode-i and mode-ii localization problems, *International Journal of Solids and Structures* 35 (1998) 4257–4274.
- [18] R. Larsson, K. Runesson, S. Sture, Embedded localization band in undrained soil based on regularized strong discontinuity—theory and fe-analysis, *International Journal of Solids and Structures* 33 (1996) 3081–3101.
- [19] J. C. Simo, J. Oliver, F. Armero, An analysis of strong discontinuities induced by strain-softening in rate-independent inelastic solids, *Computational Mechanics* 12 (1993) 277–296.
- [20] J. Oliver, Modelling strong discontinuities in solid mechanics via strain softening constitutive equations. part 1: fundamentals, *Int J Numer Methods Eng.* 39 (1996) 3575–3600.
- [21] J. Oliver, Modelling strong discontinuities in solid mechanics via strain softening constitutive equations. part 2: numerical simulation, *Int J Numer Methods Eng.* 39 (1996) 3601–3623.
- [22] R. I. Borja, A finite element model for strain localization analysis of strongly discontinuous fields based on standard galerkin approximation, *Computer Methods in Applied Mechanics and Engineering* 190 (2000) 1529–1549.
- [23] M. Jirásek, Comparative study on finite elements with embedded cracks, *Comput. Methods in Appl. Mech. Eng.* 188 (2000) 307–330.
- [24] T. Jin, H. Mourad, C. Bronkhorst, V. Livescu, Finite element formulation with embedded weak discontinuities for strain localization under dynamic conditions, *Computational Mechanics* 61 (2018) 1–16.
- [25] T. Jin, H. M. Mourad, C. A. Bronkhorst, V. Livescu, X. Zhang, C. Linder, R. A. Regueiro, Three-dimensional explicit finite element formulation for shear localization with global tracking of embedded weak discontinuities, *Computer Methods in Applied Mechanics and Engineering* 353 (2019) 416–447.
- [26] A. Ibrahimbegovic, S. Melnyk, Embedded discontinuity finite element method for modeling of localized failure in heterogeneous materials with structured mesh: An alternative to extended finite element method, *Computational Mechanics* 40 (2007) 149–155.
- [27] N. Benkemoun, M. Hautefeuille, J.-B. Colliat, A. Ibrahimbegovic, Failure of heterogeneous materials: 3d meso-scale fe models with embedded discontinuities, *International Journal for Numerical Methods in Engineering* 82 (2010) 1671 – 1688.
- [28] N. Sukumar, D. Chopp, N. Moës, T. Belytschko, Modeling holes and inclusions by level sets in the extended finite-element method, *Computer Methods in Applied Mechanics and Engineering* 190 (2001) 6183–6200.
- [29] D. Markovic, R. Niekamp, A. Ibrahimbegovic, H. Matthies, R. Taylor, Multi-scale modeling of heterogeneous structures with inelastic constitutive behaviour: Part i - physical and mathematical aspects, *Engineering Computations: Int J for Computer-Aided Engineering* 22 (2005) 664–683.
- [30] P. Hauseux, E. Roubin, D. Seyedi, J.-B. Colliat, Fe modelling with strong discontinuities for 3d tensile and shear fractures: Application to underground excavation, *Computer Methods in Applied Mechanics and Engineering* 309 (2016).
- [31] O. Stamati, E. Roubin, E. Andò, Y. Malecot, Tensile failure of micro-concrete: from mechanical tests to fe meso-model with the help of x-ray tomography, *Meccanica* 54 (2019) 707–722.
- [32] Y. Sun, Finite element modeling of the cyclic behavior of concrete : mesoscopic approaches, Ph.D.

- thesis, Université de Lille, 2019. URL: <http://ori-nuxeo.univ-lille1.fr/nuxeo/site/esupversions/80e97ee9-810c-44e1-8fc5-a9dc72d7231e>.
- [33] N. Benkemoun, R. Gelet, E. Roubin, J.-B. Colliat, Poroelastic two-phase material modeling: theoretical formulation and embedded finite element method implementation, *International Journal for Numerical and Analytical Methods in Geomechanics* 39 (2015) 1255 – 1275.
  - [34] C. Linder, D. Rosato, C. Miehe, New finite elements with embedded strong discontinuities for the modeling of failure in electromechanical coupled solids, *Computer Methods in Applied Mechanics and Engineering* 200 (2011) 141–161.
  - [35] P. Hauseux, E. Roubin, J.-B. Colliat, The embedded finite element method (e-fem) for multicracking of quasi-brittle materials, in: A. K. Shojaei, J. Shao (Eds.), *Porous Rock Fracture Mechanics*, Woodhead Publishing, 2017, pp. 177 – 196. doi:<https://doi.org/10.1016/B978-0-08-100781-5.00008-7>.
  - [36] N. Benkemoun, E. Roubin, J.-B. Colliat, Fe design for the numerical modelling of failure induced by differential straining in meso-scale concrete: Algorithmic implementation based on operator split method, *Finite Elements in Analysis and Design* 137 (2017).
  - [37] R. Borst, G. Wells, L. Sluys, Some observations on embedded discontinuity models, *Engineering Computations: Int J for Computer-Aided Engineering* 18 (2001) 241–254.
  - [38] N. Benkemoun, J.-B. Colliat, A. Ibrahimbegovic, Eléments finis enrichis pour la modélisation de la rupture des matériaux hétérogènes., in: 10e colloque national en calcul des structures, Giens, France, 2011, p. Clé USB. URL: <https://hal.archives-ouvertes.fr/hal-00592894>.